MIT Media Laboratory Perceptual Computing Group Technical Report #204

Gibbs random fields, co-occurrences, and texture modeling

I. M. Elfadel
MIT Research Lab of Electronics
50 Vassar Street
Cambridge, MA 02139
elfadel@rle-vlsi.mit.edu

R. W. Picard
MIT Media Laboratory
20 Ames Street
Cambridge, MA 02139
picard@media.mit.edu

January 15, 1993

Abstract: Gibbs random field (GRF) models and co-occurrence statistics are typically considered as separate but useful tools for texture discrimination. In this paper we show an explicit relationship between co-occurrences and a large class of GRF's. This result comes from a new framework based on a set-theoretic concept called the "aura set" and on measures of this set, "aura measures". This framework is also shown to be useful for relating different texture analysis tools: We show how the aura set can be constructed with morphological dilation, how its measure yields co-occurrences, and how it can be applied to characterizing the behavior of the Gibbs model for texture. In particular, we show how the aura measure generalizes, to any number of gray levels and neighborhood order, some properties previously known for just the binary, nearest-neighbor GRF. Finally, we illustrate how these properties can guide one's intuition about the types of GRF patterns which are most likely to form.

Index Terms – neighborhood operators, mathematical morphology, co-occurrence statistics, pattern analysis, image modeling, set theory, texture modeling, Markov random field, Gibbs distribution

1 Introduction

Almost all image processing and computer vision algorithms assume an underlying model, either explicitly or implicitly. Typically, when a Gibbs random field (GRF) is used for image restoration, segmentation, motion analysis, or texture modeling, it is used explicitly. Less well studied are the underlying models when using co-occurrence statistics or other "analysis" tools for texture discrimination. In these cases, it is not apparent what the underlying "implicit" model is. However, it should be clear that if the implicit model does not admit co-occurrences as sufficient statistics, then the ability of co-occurrence based features to distinguish the analyzed textures will eventually fail.

Whether an image model is implicit or explicit, it is important to be able to evaluate the model's inherent advantages and limitations. Although theoretical in its tools, this type of investigation is practical in its implications, for it allows to predict the performance of pattern analysis algorithms beyond the typically small set of standard test data. In this paper, we describe such an investigation for the class of GRF models first introduced by Besag [1], and subsequently used in [2, 3] for texture analysis and synthesis. Our investigation is far from complete, but the approach that we use will illustrate how the capabilities of a given model can be analyzed irrespective of the application domain. Thus, the results that we have obtained should aid all applications of this class of GRF's.

While studying the behavior of the GRF, we developed an intermediate representation which facilitated many of our results. The new representation is based on set theory and leads to an intuitive analogy between gray levels coloring the pixels of a texture and fluids mixing and separating in a multi-component solution. The primary tools of this new representation, the "aura set" and "aura measure", are defined in Section 2. The name "aura" comes from the "surrounding" shape of the set it describes.

A bit of justification is called for when one claims to introduce yet another new set of tools. As will be shown, these tools are not really "new" in the sense of being independent of known techniques. Rather, they are new in their sense of application, namely, to establish relationships between morphology, co-occurrences, and Gibbs random fields. Nor should one expect that they would automatically be suitable for unifying a larger set of texture analysis methods. Building a foundation within which the twenty or so existing texture tools can be evaluated is one of our long-term goals, but the results reported here are at best a small component.

The contributions of this paper can be summarized as follows. First, we develop the set-theoretic framework which includes the "aura set" and "aura measure", and establish its construction from morphology. Second, we relate the aura measure to gray-level co-occurrences, a tool well known in texture discrimination. Third, we apply the new tools to the Gibbs random field model. The Gibbs energy is rewritten as a linear combination of the aura measures, and hence of co-occurrences. Fourth, we use the aura measures to draw an analogy between gray levels and fluids. We make this analogy to provide the reader with some intuition into what kinds of patterns the model is likely to form. Finally, we describe how the relations among the aura measures change as the Gibbs energy is minimized, and the implications this has for pattern formation, especially in the context of maximum a posteriori (MAP) estimation.

2 Morphology and Auras

2.1 Notation, Definitions, and Properties

We consider a finite lattice $\mathcal{S}$ with a neighborhood structure $\mathbf{N} = \{\mathcal{N}_s, s \in \mathcal{S}\}$, where every $\mathcal{N}_s$ is a subset of the lattice $\mathcal{S}$. The number of elements of a subset $A \subseteq \mathcal{S}$ will be denoted by $|A|$. The following definition is basic to the new framework.

Definition 1 *Let A, B be two subsets $\subseteq \mathcal{S}$. Then the aura of A with respect to B for the neighborhood structure $\{\mathcal{N}_s, s \in \mathcal{S}\}$ is a subset of $\mathcal{S}$ defined by*

$$\bigcup_{s \in A} (\mathcal{N}_s \cap B). \tag{1}$$

The aura of a set A with respect to a set B will be denoted by

$$\mathcal{O}_B(A, \mathbf{N}). \tag{2}$$

The aura of a set with respect to itself will be called the self-aura.

It is very important to note that the aura depends on the neighborhood structure chosen for the lattice. All the results derived in this paper are valid for any choice of the $\mathcal{N}_s$'s, including "non-nearest neighbors". In all the derivations, the structure $\mathbf{N}$ is assumed to be given once and for all. Thus, we choose to omit the notational dependency on $\mathbf{N}$ from (2) and use for the aura the simplified notation $\mathcal{O}_B(A)$.

Note that in principle the neighborhood can be site-dependent. (This is often the assumption when dealing with boundary conditions in images.) However, when the finite lattice is rectangular and has

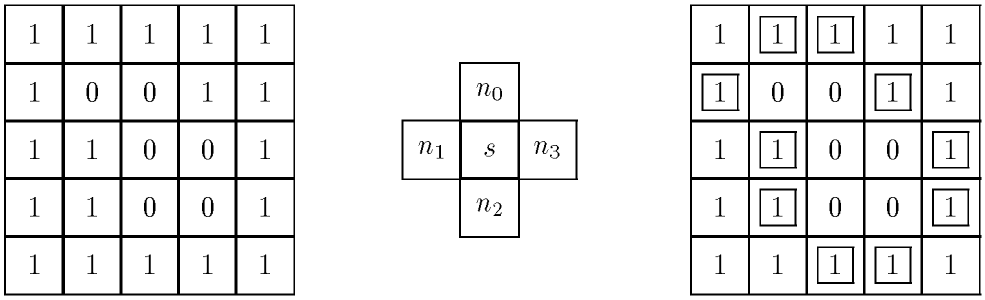

(a) (b) (c)

Figure 1: Example of an aura on a binary lattice with the four nearest-neighbors. (a) Sample binary lattice. (b) Neighborhood structure of four nearest-neighbors, n_i, of a lattice site s. (c) The set of double-boxed sites is the aura of the set of all 0's with respect to the set of all 1's. Notice the "aura-like" shape from which the set takes its name.

---

the periodic boundary conditions, where the top is connected to the bottom, and the left to the right, then the $\mathcal{N}_s$'s will be assumed to be the translates of a basic neighborhood, denoted $\mathcal{N}$. We name $\mathcal{N}$ a *structuring element*, after the terminology of mathematical morphology. In this case, the number of elements of each neighborhood, $|\mathcal{N}_s|$, is constant and equal to $|\mathcal{N}|$. When boundary conditions other than periodic are made, then care should be taken in the definition of the neighborhoods of the sites that lie on the lattice boundaries. In particular, the size of the neighborhood will vary along the boundaries and will differ from the size of the inner site neighborhoods.

Example 2 *An example of an aura is shown in Figure 1. In (a) is shown a binary* 5×5 *lattice,* $\mathcal{S}$*. Let* $A = \{a \mid a \in \mathcal{S}, a = 0\}$ *and* $B = \{b \mid b \in \mathcal{S}, b = 1\}$*. Let* $\mathcal{N} = \{n_i,\ i = 0,\ 1,\ 2,\ 3\}$ *as shown in (b). Then* $\mathcal{O}_B(A)$ *are the elements marked by the double-boxes in (c).*

Several theoretical properties of the aura set are listed in Appendix A.

2.2 Mathematical Morphology Formulation of Aura

Mathematical morphology has been applied to a rapidly expanding variety of image processing tasks including nonlinear filtering, pattern analysis, and fractal dimension estimation [4]. In this section we show how the aura set can be constructed using a simple morphological operation. For $A, B \subseteq \mathcal{S}$, we consider only the case $A \cap B = \emptyset$. This is true in image processing when the site values correspond to image gray levels.

Following the notation of [4], we give the following definition from mathematical morphology:

Definition 3 *Let* A *and* B *be two sets. Then the dilation, denoted by* $\oplus$*, of* A *by* B *is*

$$A \oplus B = \{a + b \mid a \in A,\ b \in B\} = \bigcup_{b \in B} A_b\ . \tag{3}$$

We say A_b is the *translate* of the set A by the vector b. Note that $A \oplus B = B \oplus A$. If $\hat{B}$ represents the set B after planar rotation by 180°, then $A \oplus B = \{z \mid (\hat{B} + z) \cap A \neq \emptyset\}$, i.e., the set of points where translated $\hat{B}$'s intersect A.

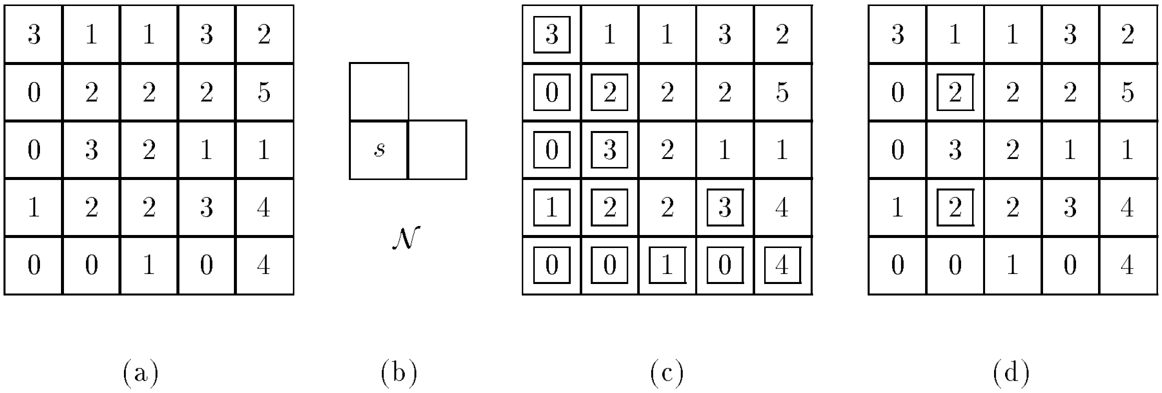

Figure 2: Example of forming an aura using morphological dilation. (a) Graylevel lattice. (b) Structuring element, $\mathcal{N}$. (c) The double-boxed sites are the dilation of the set of all 0's with $\mathcal{N}$. (d) The double-boxed sites are the aura of the 0's with respect to the 2's.

Now, we form the aura of A with respect to B in terms of dilation:

$$\begin{aligned} \mathcal{O}_B(A) &= \bigcup_{a \in A} (\mathcal{N}_a \cap B) \\ &= (\bigcup_{a \in A} \mathcal{N}_a) \cap B \\ &= (\mathcal{N} \oplus A) \cap B \end{aligned} \tag{4}$$

where $\mathcal{N}$ is the structuring element of which the neighborhoods $\mathcal{N}_a$ are the translates. Thus we have that the aura of A with respect to B on a lattice with neighborhood structure $\mathbf{N}$ is equivalent to the dilation $\mathcal{N} \oplus A$ followed by intersection with B. Those familiar with mathematical morphology may wish to note that we construct a gray-level aura set using binary dilation.

Example 4 *In Figure 2 we show an example of forming an aura using dilation. In (a) is shown a* 5×5 *lattice,* $\mathcal{S}$*, in which the sites are assigned the values* $0, 1, 2, 3, 4,$ *and* 5*. Let* $A = \{a \mid a \in \mathcal{S},\ a = 0\}$ *and* $B = \{b \mid b \in \mathcal{S},\ b = 2\}$*. Let* $\mathcal{N}$ *be the structuring element as shown in (b). The dilation,* $A \oplus \mathcal{N}$ *is given in (c). Intersecting this set with* B *gives the aura with respect to* B*,* $\mathcal{O}_B(A)$*, shown in (d).*

3 The Measure of an Aura

3.1 Definitions and Properties

The easiest way for measuring the size of the aura of a set A with respect to a set B is by counting the number of elements, $|\mathcal{O}_B(A)|$. Note that we have, from the definition and known properties of sets,

$$|\mathcal{O}_B(A)| \leq \sum_{s \in A} |\mathcal{N}_s \cap B|. \tag{5}$$

In problems involving image synthesis or processing, it is the right side that appears more frequently. In particular, we will show that the right side relates to image co-occurrence statistics. It also turns out that the right side is a better measure of how "broken" the boundary of the set A is. For these reasons, the following definition of the measure of an aura is adopted:

Definition 5 *The aura measure, denoted by $m(A, B)$, is defined by*

$$m(A, B) = \sum_{s \in A} |\mathcal{N}_s \cap B|. \tag{6}$$

Example 6 *For the sets in Example 2, $m(A, B) = 12$, and $|\mathcal{O}_B(A)| = 10$.*

The properties necessary for the "aura measure" to be a valid set "measure" are listed in Appendix A.

Note that, in general, $m(A, B) \neq m(B, A)$. However, there is a property that says when the neighborhood structure is symmetric, then there is an equality. First, let us define a symmetric neighborhood structure.

Definition 7 *A neighborhood structure* $\mathrm{N} = \{\mathcal{N}_s, s \in \mathcal{S}\}$ *is symmetric if*

$$\forall s, r \in \mathcal{S}, \qquad s \in \mathcal{N}_r \text{ if and only if } r \in \mathcal{N}_s. \tag{7}$$

Example 8 *An example of a symmetric neighborhood structure is shown in Figure 1(b). An example of a non-symmetric neighborhood structure is shown in Figure 2(b).*

Note that causal and semicausal neighborhoods are never symmetric. On the other hand, in applications employing Markov/Gibbs random fields, the neighborhoods are noncausal and must be symmetric. A symmetric neighborhood structure is also called a "neighborhood system" by Geman and Geman [5]. The next proposition, proved in Appendix B, states the equivalence between aura measure symmetry and neighborhood symmetry.

Proposition 9 *The following two conditions are equivalent:*

i) $\{\mathcal{N}_s, s \in \mathcal{S}\}$ *is a symmetric neighborhood structure;*

ii)

$$m(A, B) = m(B, A), \qquad \forall A, B \subseteq \mathcal{S}. \tag{8}$$

It is important to note that the second condition must be satisfied for *any* two subsets A and B of $\mathcal{S}$. It is not difficult to construct examples of *particular* subsets A and B such that (8) is satisfied, but the neighborhood is not symmetric. For instance, two white (A) and black (B) stripes that partition a binary, periodic, square lattice in which every pixel has only one neighbor to its right is such that $m(A, B) = m(B, A)$, but the neighborhood is clearly not symmetric. There are two extreme cases that are worth mentioning. The first is when every site in the lattice is its only neighbor. In this case, we have $\mathcal{N}_s = \{s\}$, and for any two sets $A, B \subseteq \mathcal{S}$, $m(A, B) = m(B, A) = |A \cap B|$. The second extreme case is when the neighborhood of each site is the whole lattice, i.e., $\forall s \in \mathcal{S}, \mathcal{N}_s = \mathcal{S}$. Then for any two subsets $A, B \subseteq \mathcal{S}$, we have $m(A, B) = m(B, A) = |A||B|$.

3.2 Aura Measures, Boundary Length, and Graph Theory

When the lattice is equipped with the four nearest neighbor structure, then the aura measure of two sets A and B becomes the boundary length (computed in number of pixels) between A and B. The boundary length property has several useful interpretations. In this section we describe relationships to the Ising model of statistical mechanics, to fluid mechanics, and to graph-theoretic concepts.

Measuring the boundary length leads to an intuitive explanation of the behavior of the well-known binary Ising model of statistical mechanics [6]. This model consists of interacting spins on a binary lattice with the four nearest neighbor structure. There are two types of spins, up and down, to whose sites we associate the sets A and B, respectively. The Ising model operates so as to minimize an energy function which is essentially $m(A, B)$. In the case of "spontaneous magnetization", where all spins are oriented the same way, either all up or all down, then the boundary between A and B is minimized by being set to zero. Thus, the lattice becomes full of elements of A or full of elements of B. The opposite case, where $m(A, B)$ is maximized, corresponds to the antiferromagnetic state. This is the checkerboard pattern, where spins alternate and the boundary between A and B is maximized.

The cases of ferromagnetism and antiferromagnetism in the Ising model are also analogous to the separation and mixing of two fluids [7]. In aura notation, the miscibility of two fluids is represented by $m(A, B)$ [1]. For immiscible fluids $m(A, B)$ is minimized; for miscible, $m(A, B)$ is maximized. When $m(A, B)$ is normalized over some unit area (or more typically for fluids, unit volume), it gives a measure of the interfacial energy driving the separation of the two phases A and B [8]. Since the aura measure is valid on a general lattice with any number of fluids $A_i, i = 0, 1, \ldots, n-1$, and any neighborhood structure, it generalizes both the boundary length and miscibility concepts.

Aura measures can similarly be related to the edge boundaries of graph theory. Any lattice $\mathcal{S}$ equipped with a *symmetric* neighborhood structure $\{\mathcal{N}_s, s \in \mathcal{S}\}$ can be considered an undirected graph $G(V, E)$ where V, the set of vertices, is identical to the set of lattice sites, $\mathcal{S}$, and the set of edges, E, is given by the set of the lattice links that connect the lattice sites to their neighbors, according to the neighborhood structure defined on the lattice. The *degree* of each vertex, i.e., the number of times this vertex is used as an endpoint for the graph edges, is equal to its neighborhood size. When the neighborhood size is independent of the site, all the graph vertices have the same degree.

Continuing the analogy, let A be a subset of graph vertices. Then the set of the graph edges linking the vertices of A to the vertices of A^c, the complementary set of A, is called the *edge boundary* of A [9]. The number of these edges can be considered a measure of the edge boundary length. This number is also identical to $m(A, A^c)$, the aura measure of the subset A with respect to its complementary set A^c. If B is another subset of vertices disjoint from A, i.e., $B \subseteq A^c$, then $m(A, B)$ can be considered as the length of that part of the edge boundary of A that is shared with the subset B. The aura measure is therefore a slight but useful generalization of the concept of an edge boundary in a graph. Indeed, the optimization problems used in texture synthesis can be interpreted as generalized isoperimetric problems [9] defined on the graph underlying the image lattice, as we will see in Appendix G.

Computing invariants is an important goal of pattern recognition. This interpretation of the aura measure in terms of edge boundary allows us to conclude that the aura measure is invariant under all graph isomorphisms [10] applied to the graph defined by the lattice and the neighborhood structure. Notice that these isomorphisms include not only lattice rotations but also all lattice "distortions" that keep invariant the neighborhood structure.

3.3 Aura Measures and Exchange Operations

Many algorithms in combinatorial and graph optimization are based on an operation in which an element of a given set is exchanged with an element from another set. For example, 1-D algorithms such as Quicksort exchange elements to order a list. In 2-D, Monte Carlo algorithms such as the classical Metropolis method attempt to exchange values between pairs of sites in an effort to minimize the energy of the system. Such methods are finding increasing use in image processing, especially through the use of simulating annealing [11]. The effect of exchange operations on the measures of aura sets is derived in Appendix F.

Please note: For the rest of the paper, we will assume that the finite lattice is rectangular with periodic boundary conditions. The neighborhoods of the lattice are assumed to be the translates of a structuring element $\mathcal{N}$. These are standard assumptions in the literature, which serve to simplify neighborhood

[1] For two fluids, one would expect the boundary between them would not depend on the side from which it was measured – hence one could intuitively expect $m(A, B) = m(B, A)$.

notation without affecting any of the main results of this paper.

3.4 Aura Measures on Subneighborhoods

Most natural textures contain anisotropy. When modeling such patterns, e.g., with the anisotropic Markov models considered in Section 5, it is desirable to define a function that varies within a neighborhood. This function will be constant on a given *subneighborhood*, $\mathcal{N}_s^k \subseteq \mathcal{N}_s$. If there are K such subneighborhoods, then

$$\mathcal{N}_s = \bigcup_{k=1}^{K} \mathcal{N}_s^k, \quad \forall s \in \mathcal{S}, \tag{9}$$

where $\mathcal{N}_s^k \cap \mathcal{N}_s^l = \emptyset, \quad \forall l \neq k$. Then we can define the aura of A with respect to B for the k-th subneighborhood structure by

$$\mathcal{O}_B^k(A) = \bigcup_{s \in A} (B \cap \mathcal{N}_s^k). \tag{10}$$

It can be readily seen using the above definition that

$$\mathcal{O}_B(A) = \bigcup_{k=1}^{K} \mathcal{O}_B^k(A). \tag{11}$$

The aura measure of the k-th subneighborhood will simply be

$$m^k(A, B) = \sum_{s \in A} |\mathcal{N}_s^k \cap B|. \tag{12}$$

Since the K subneighborhoods $\mathcal{N}^k$ partition $\mathcal{N}$ we can easily see that

$$m(A, B) = \sum_{k=1}^{K} m^k(A, B), \tag{13}$$

In the next section, we will see how the above equation allows us to relate aura measures for gray-level sets to co-occurrences.

4 Aura Measures and Co-Occurrences

4.1 The Aura Matrix of a Partition

We now introduce a useful tool for pattern processing applications, the *aura matrix*. The aura matrix is a representation of the aura measures for all the sets of interest on the lattice. Here we define it for sets which partition the lattice, as is the case for gray-level sets in images:

Definition 10 *Let $\{S_i, 0 \leq i \leq n-1\}$ be a partition of $\mathcal{S}$, i.e., $S_i \subseteq \mathcal{S}$, $i = 0, 1, \ldots, n-1$, $\bigcup_{i=0}^{n-1} S_i = \mathcal{S}$ and $S_i \cap S_j = \emptyset$ unless $i = j$. Then the aura matrix, $\mathbf{A}$, is the $n \times n$ integer matrix defined by $\mathbf{A} = [a_{ij}]$ where $a_{ij} = m(S_i, S_j)$, $0 \leq i, j \leq n-1$.*

The proof of the following proposition is given in Appendix C.

Proposition 11 *(Aura Matrix Properties) Let $\mathbf{A}$ be an aura matrix. Then,*

(a) Each row sum satisfies:

$$\sum_{j=0}^{n-1} a_{ij} = |S_i||\mathcal{N}|, \; i = 0, \ldots, n-1;$$

(b) Each column sum satisfies:

$$\sum_{i=0}^{n-1} a_{ij} = |S_j||\mathcal{N}|, \ j = 0, \ldots, n-1;$$

(c) If $\mathcal{N}$ is symmetric, then $\mathbf{A}$ is symmetric, and

$$\sum_{j=0}^{n-1} a_{kj} = \sum_{i=0}^{n-1} a_{ik} = |S_k||\mathcal{N}|, \ \ k = 0, \ldots, n-1;$$

If we did not assume periodic boundary conditions, then the right-hand sides would become upper bounds on the left-hand sides in (a)-(c). In Section 5, these properties are used for defining constraints on aura measures in images.

Example 12 *Consider a checkerboard arrangement on the lattice, where sites alternate between 0 (black) and 1 (white). Assume a four nearest neighbor structure, and let S_0 be the subset of sites colored black and S_1 be the subset colored white. Then the aura matrix is*

$$\mathbf{A} = 2|\mathcal{S}| \begin{pmatrix} 0 & 1 \\ 1 & 0 \end{pmatrix}. \tag{14}$$

Note that all entries in $\mathbf{A}$ are always positive, but $\mathbf{A}$ is not necessarily positive semi-definite, e.g., $(1,-1)\mathbf{A}(1,-1)^T = -2$. This contrasts with a correlation matrix, which is positive semi-definite.

Assume now that to each site s of the lattice $\mathcal{S}$, there is assigned an integer $x_s \in \Lambda = \{0, 1, \ldots, n-1\}$ which represents the gray-level value of a pixel at site s. The gray level sets of the lattice are defined as follows:

$$\mathcal{S}_g = \{s \in \mathcal{S} | x_s = g\}, \ \forall g \in \Lambda. \tag{15}$$

It is clear that the gray-level subsets $\mathcal{S}_g, g \in \Lambda$, constitute a partition of $\mathcal{S}$. To simplify notation, we denote the aura measure of the gray-level set $\mathcal{S}_g$ with respect to the gray-level set $\mathcal{S}_{g'}$ by $m(g, g')$, instead of the more cumbersome $m(\mathcal{S}_g, \mathcal{S}_{g'})$. These measures also define an aura matrix $\mathbf{A} = [a_{gg'}] = [m(g, g')]$.

For images of uniformly distributed pseudorandom noise, using a variety of symmetric neighborhood structures, we have observed for $g, g' = 0, 1, \ldots, n-1$, that $a_{gg'}$ is constant. This is consistent with a uniform probability distribution for the noise and indicates perfect mixing (in the fluids analogy) between gray levels. The following sections explore the connections of the gray-level aura matrix with both the co-occurrence matrix and the covariance matrix. Moreover a probabilistic interpretation of the aura matrix will be given.

4.2 Relationship of Aura Matrix to Co-occurrence Matrix

The significance of pairwise gray-level information for visual texture discrimination was advocated in 1962 by Julesz [12]. Since then, co-occurrence matrices and features derived from them have become a very popular tool for a variety of practical texture analysis problems [13, 14].

Definition 13 *Let $\mathbf{d}$ be a lattice vector and let $C_{gg'}(\mathbf{d})$ be the set of site pairs defined by*

$$C_{gg'}(\mathbf{d}) = \{(s, r) \in \mathcal{S} \times \mathcal{S}, \ \textit{such that} \ s - r = \mathbf{d}, \ x_s = g, \ x_r = g'\}, \tag{16}$$

and let $c_{gg'}(\mathbf{d})$ denote the number of elements of $C_{gg'}(\mathbf{d})$. Then the co-occurrence matrix is defined by $\mathbf{C}(\mathbf{d}) = [c_{gg'}(\mathbf{d})]$.

Note that when $\mathcal{N}_s = \{s + \mathbf{d}\}$ then $c_{gg'}(\mathbf{d}) = m(g, g')$ and $\mathbf{C}(\mathbf{d}) = \mathbf{A}$. It follows that when the site neighborhood consists of one element, the aura matrix and the co-occurrence matrix are identical. In general, the aura matrix is equivalent to a sum of co-occurrence matrices, taken over the displacements contained in the neighborhood structuring element. Indeed, if we make the neighborhood obtained from a displacement along the vector $\mathbf{d}_k$ identical to the $\mathcal{N}^k$ subneighborhood of $\mathcal{N}$, then we have $c_{gg'}(\mathbf{d}_k) = m^k(g, g')$. Using Equation (13), we can write

$$m(g, g') = \sum_{k=1}^{K} m^k(g, g') = \sum_{k=1}^{K} c_{gg'}(\mathbf{d}_k). \tag{17}$$

Co-occurrence displacements are often defined in terms of angle and distance, instead of vectors, thus giving a symmetric co-occurrence matrix. This is equivalent to an aura matrix with the corresponding two-neighbor symmetric $\mathcal{N}_s$. In [15] co-occurrences were generalized to provide statistics of features instead of just gray levels. The same can be easily done with the aura matrix, providing "mixing" and "clumping" measures for any pattern feature.

In all these cases, the aura matrix generalizes the pairwise co-occurrence matrix by allowing the counts to occur over any geometry. Thus, it gives us a cohesive and notationally appealing framework for forming combined co-occurrence matrices similar to the ones considered in Rosenfeld and Kak [16]. Combining co-occurrences is important for reducing the large number of features contained in the matrices. Rosenfeld and Kak also found that the combination of co-occurrences along more than one displacement vector were better for texture discrimination when texture directionality was not important. A more recent work with similar implications is [17] where the texture descriptors are made from a combination of pairwise co-occurrences, which is equivalent to an aura matrix with the eight nearest neighbors structure. Why have researchers found it better to combine the co-occurrence statistics over what is actually a Gibbs/Markov neighborhood? We suggest that the answer to this resides in the relationship between co-occurrences and aura measures on the one hand, and between aura measures and the Gibbs probability distribution on the other. This latter relationship will be explicitly made in Section 5.

4.3 Relationship of Aura Matrix to Covariance Matrix

The aura measures and co-occurrences have a special relation to the auto-correlation even though they are different. For one thing, the aura and co-occurrence matrices have a dimensionality determined by the number of gray levels, while the auto-correlation matrix dimensionality is given by the image size. Moreover aura and co-occurrence matrices need not be positive semidefinite like auto-correlation matrices. In tests by Conners and Harlow comparing discrimination abilities of texture analysis tools [18], the co-occurrences performed much better than the power spectrum, which is the Fourier transform of the auto-correlation. Conners and Harlow concluded that the co-occurrences contain more "textural information" than the correlations.

The relationship between co-occurrences and correlation is not new, but is shown here in our notation for demonstrating the general application of the aura notation. To compute the autocorrelation at a given lag, $\mathbf{d}$, we form the sum of products,

$$\sum_{s \in \mathcal{S}} x_s x_{s+\mathbf{d}}.$$

This can be equivalently written as

$$\sum_{g \in \Lambda} \sum_{s \in \mathcal{S}_g} g x_{s+\mathbf{d}}$$

or

$$\sum_{g \in \Lambda} \sum_{s \in \mathcal{S}_g} g \sum_{g' \in \Lambda} g' \sum_{(s+\mathbf{d}) \in \mathcal{S}_{g'}} 1.$$

Regrouping and evaluating the right-most sum gives

$$\sum_{g,g'\in\Lambda} gg' \sum_{s\in\mathcal{S}_g} |(s+\mathbf{d})\cap\mathcal{S}_{g'}|,$$

which by the definition of co-occurrence reduces to

$$\sum_{g,g'\in\Lambda} gg' c_{gg'}(\mathbf{d}). \tag{18}$$

Thus the correlation at a particular lag, $\mathbf{d}$, is the weighted sum of co-occurrences at the displacement $\mathbf{d}$.

Similarly, we can define the neighborhood-based correlation for a given neighborhood structure as

$$\sum_{s\in\mathcal{S}} \sum_{r\in\mathcal{N}_s} x_s x_r.$$

Then following the same steps as for the co-occurrence case, we can show that

$$\sum_{g,g'\in\Lambda} gg' m(g,g') \tag{19}$$

is also a weighted sum of aura measures. This sum will show up again in Section 5.

In the next section we will give another interpretation of aura matrices linking them to neighborhood-based gray-level transition probabilities.

4.4 The Normalized Aura Matrix – Probabilistic Interpretation

Like the co-occurrence matrix, the aura matrix is easily converted to a stochastic matrix. In this section we consider its probabilistic interpretation.

We assume in this section that $\mathcal{N}_s$ is symmetric, $|\mathcal{N}_s| = \nu$, and that $|S_g| = |\mathcal{S}|/n = \gamma$, $g = 0, \ldots, n-1$. This is the uniform histogram case, which is the maximum entropy prior when no information is known about the initial distribution. We define the normalized aura matrix, $\mathbf{M}$, by

$$\mathbf{M} = \frac{1}{\gamma\nu}\mathbf{A}, \tag{20}$$

and refer to it as the *miscibility matrix.* The miscibility matrix $\mathbf{M}$ satisfies Proposition 11 with the additional property that the rows and columns of $\mathbf{M}$ now sum to 1. Therefore $\mathbf{M}$ is doubly stochastic.

The elements of $\mathbf{M}$, called the *miscibility measures*, $\mathbf{m}(g,g') = m(g,g')/\gamma\nu$, can be given a probabilistic interpretation. Indeed, as in the transition matrix of a Markov chain, the coefficient $\mathbf{m}(g,g')$ can be interpreted as the *conditional probability* $p_{gg'}$ that a given site of color g' has in its neighborhood a site of color g. Note that these conditional probabilities depend on the neighborhood geometry and size. They can be interpreted as neighborhood-based gray-level transition probabilities. They differ from the probabilities defined in [16] in that they do not depend on the image scan direction. With this probabilistic interpretation, we can write the correlation, covariance, and correlation coefficients of the lattice site values.

We let g, g', and g'' be three gray-level values. The gray-level correlation is given by

$$R(\nu) = \sum_{0\le g,g'\le n-1} gg' p_{gg'} p_{g'}, \tag{21}$$

where $p_{g'}$ is the probability of a given pixel to have the gray-level value g'. Since we have assumed the histogram uniform this probability is equal to $\frac{1}{n}$. Therefore the correlation can be written

$$R(\nu) = \frac{1}{n} \sum_{0\le g,g'\le n-1} gg' p_{gg'}. \tag{22}$$

The gray-level covariance is given by

$$C(\nu) = \frac{1}{n} \sum_{0 \le g, g' \le n-1} (g - \overline{g})(g' - \overline{g}) p_{gg'}, \tag{23}$$

where $\overline{g}$ is the mean of the gray-level values. When the histogram is uniform the mean is given by

$$\overline{g} = \frac{1}{n} \sum_{g=0}^{n-1} g = \frac{n-1}{2}.$$

The variance σ^2 of the gray levels can be calculated from

$$\sigma_g^2 = \frac{1}{n} \sum_{g=0}^{n-1} (g - \overline{g})^2 = \frac{(n-1)(n+1)}{12}.$$

Knowing the variance and the covariance, we can compute the gray-level correlation coefficient by

$$\rho(\nu) = \frac{C(\nu)}{\sigma^2}.$$

Note that $R(\nu)$, $C(\nu)$, and $\rho(\nu)$ depend on the neighborhood geometry and size. The neighborhood size was used as an argument for these quantities to emphasize this dependence.

A natural question to ask is how do the statistical quantities defined in the previous paragraph vary as we change the neighborhood structure from $\{\mathcal{N}_s,\ s \in \mathcal{S}\}$ to $\{\mathcal{N}'_s,\ s \in \mathcal{S}\}$, such that $\mathcal{N}_s \subset \mathcal{N}'_s,\ \ \forall s \in \mathcal{S}$? Under a rather mild assumption on the new neighborhood structure, we can obtain a closed form relationship between $R(\nu)$ and $R(\nu')$, $C(\nu)$ and $C(\nu')$, and $\rho(\nu)$ and $\rho(\nu')$, where $\nu' = |\mathcal{N}'_s|$.

Let $p'_{gg'}$ be the coefficients of the miscibility matrix $\mathbf{M}'$ of the new neighborhood structure. The objective is to find a relationship between $p_{gg'}$ and $p'_{gg'}$. From the probabilistic interpretation we have

$$p'_{gg'} = \Pr(\exists r \in \mathcal{N}'_s, x_r = g | \exists s \in \mathcal{S}, x_s = g').$$

Since $\mathcal{N}_s \subset \mathcal{N}'_s$, the site r neighboring s could be either in $\mathcal{N}_s$ with probability κ equal to the ratio of the neighborhood sizes, i.e., $\kappa = \frac{\nu}{\nu'}$, or in $(\mathcal{N}'_s - \mathcal{N}_s)$ with probability equal to $1 - \kappa$. It follows that

$$\begin{aligned} p'_{gg'} &= \kappa \Pr(\exists r \in \mathcal{N}_s, x_r = g | \exists s \in \mathcal{S}, x_s = g') \\ &+ (1-\kappa) \Pr(\exists r \in (\mathcal{N}'_s - \mathcal{N}_s), x_r = g | \exists s \in \mathcal{S}, x_s = g'). \end{aligned} \tag{24}$$

The first probability in the above equation is simply $p_{gg'}$, whereas the second will be shown to depend in a simple manner on the matrix $\mathbf{M}$ of the old neighborhood structure. To accomplish this, let us assume that the neighborhood $\mathcal{N}'_s$ is larger than $\mathcal{N}_s$ but not much larger. Formally we will assume that

$$\forall r \in (\mathcal{N}'_s - \mathcal{N}_s),\ \ \mathcal{N}_r \cap \mathcal{N}_s \neq \emptyset. \tag{25}$$

Note that using mathematical morphology, this assumption can be equivalently stated:

$$\mathcal{N}'_s \subseteq \mathcal{N}_s \oplus \mathcal{N}\ . \tag{26}$$

Let q be an element of this nonempty intersection, and let $x_q = g''$ be its gray-level value. Note that x_q can take any value between 0 and $n-1$, and that $r \in \mathcal{N}_q$, since the neighborhood structure is symmetric.

Therefore the second probability in the $p'_{gg'}$ equation can be written as

$$\sum_{g''=0}^{n-1} \Pr(\exists r \in \mathcal{N}_q, x_r = g | \exists q \in \mathcal{N}_s, x_q = g'') \Pr(\exists q \in \mathcal{N}_s, x_q = g'' | \exists s \in \mathcal{S}, x_s = g').$$

From the definition of the coefficients of the matrix $\mathbf{M}$, we can see that the above summation is exactly

$$\sum_{g''=0}^{n-1} p_{gg''}p_{g''g'}, \tag{27}$$

which is nothing but the (g, g') coefficient of the matrix $\mathbf{M}^2$. The previous calculation can be summarized compactly in the following equation

$$\mathbf{M}' = \kappa\mathbf{M} + (1-\kappa)\mathbf{M}^2, \tag{28}$$

which says that under assumption (25) the miscibility matrix of the new neighborhood structure is a convex combination of the miscibility matrix of the old neighborhood structure and its square. Knowing the matrix $\mathbf{M}'$, we can compute the statistical quantities described earlier. In particular, we have for the correlation coefficient

$$\rho(\nu') = \kappa\rho(\nu) + (1-\kappa)\rho_2(\nu),$$

which is also a convex combination of the "short range" correlation coefficient $\rho(\nu)$ and the "long-range" correlation coefficient $\rho_2(\nu)$ that results from the transition matrix $\mathbf{M}^2$. One possible application of (28) is to the study of the multiscale behavior of the gray-level transition probabilities.

5 Application to Gibbs Texture Modeling

5.1 Background and motivation

Causal 1-D Markov models have a long history of usefulness for many image processing applications. Since the establishment of the equivalence between Markov and Gibbs random fields there has been renewed emphasis on their noncausal 2-D versions. In particular, the GRF's have been explored for the representation of natural texture patterns [19, 3, 20, 21, 22]. The assumption that the GRF can model image textures has also been used to justify GRF models in image compression, classification, restoration, and segmentation [23, 5, 24, 25].

In the last two applications, GRF models fit naturally within the Bayesian paradigm of MAP estimation, where the objective is to find an estimate $\hat{\mathbf{x}}$ of the original image $\mathbf{x}$ that solves the maximization problem,

$$\max_{\mathbf{x}} P(\mathbf{x}|\mathbf{y}) = \max_{\mathbf{x}} \frac{P(\mathbf{y}|\mathbf{x})P(\mathbf{x})}{P(\mathbf{y})}.$$

In the above formula, $\mathbf{y}$ is the corrupted image, $P(\mathbf{x})$ and $P(\mathbf{y})$ are the probability distributions of the original and corrupted images, respectively, while $P(\mathbf{x}|\mathbf{y})$ is the conditional probability distribution of the original image given the data. Note that while $P(\mathbf{y})$ is irrelevant to the above maximization problem, the *a priori* assumption on the original image as given by the distribution $P(\mathbf{x})$ is essential. Note also that when the corrupted image is too noisy, the dependence of $\mathbf{y}$ on the original image $\mathbf{x}$ is weak, so that one can write

$$P(\mathbf{y}|\mathbf{x}) \approx P(\mathbf{y}),$$

and the MAP estimation becomes a maximization of the *a priori* probability distribution of the original image. Beside being one of the main motivations behind this paper, this fact also motivates our consideration of the minimum-energy configurations of the Gibbs distribution as will be explained in Section 5.2.

Another important motivation is that of texture synthesis. When textures are modeled explicitly using GRF models, a textural pattern is synthesized by using statistical sampling from the distribution $P(\mathbf{x})$. Using the neighborhood-based framework developed in the previous sections, we will show how we can relate the sampled texture patterns to physical ideas such as mixing, separation, and boundary optimization in multiphase fluids.

5.2 The GRF Approach to Texture Synthesis

The basic methodology for GRF texture synthesis is the following. Let $\mathbf{x}$ be the vector $(x_s, 1 \le s \le |\mathcal{S}|)$ of site gray-level values and Ω be the set $\Lambda^{|\mathcal{S}|}$ of all possible configurations taken by $\mathbf{x}$. For the finite periodic lattice $\mathcal{S}$, with the symmetric neighborhood structure $\{\mathcal{N}_s, s \in \mathcal{S}\}$, we define the Gibbs energy

$$E(\mathbf{x}) = \sum_{s \in \mathcal{S}} V_s(x_s) + \sum_{s \in \mathcal{S}} \sum_{r \in \mathcal{N}_s} V_{sr}(x_s, x_r), \tag{29}$$

where the V_s's are the single-site potentials and the V_{sr}'s are the two-site potentials [2]. In the physics literature the single-site potentials are called the external field while the two-site potentials define the interaction of the so-called internal field. At this stage we would like to make the following two remarks:

(1) Equation (29) is not the most general expression for the Gibbs energy. Interactions in which more than two sites are involved can also be considered. In this paper, we restrict ourselves to models having only two site interactions, precisely because they are the ones compatible with co-occurrence statistics. In fact, the co-occurrences are sufficient statistics for these models. We refer to the work of [26] for the case of textures with higher-order interaction models.

(2) The external field in (29) can be used to represent input data such as the noisy image in the smoothing and segmentation problem. The relative importance of the potentials associated with the external and internal field reflects, in this case, our confidence in the sensors and the prior model. As was mentioned in the previous section, our results are particularly relevant in the case when the sensors are very noisy.

To the Gibbs energy, thus defined, we can assign a random field whose probability distribution is given by

$$P(\mathbf{x}) = \frac{1}{Z} \exp\left(-\frac{1}{T} E(\mathbf{x})\right), \tag{30}$$

where T is the "temperature" of the field and Z is a positive normalizing constant, also known in the physics literature as a partition function. It is not difficult to prove that the above joint probability distribution defines a Markov random field with respect to the neighborhood structure $\{\mathcal{N}_s, s \in \mathcal{S}\}$ [5].

A textural pattern is obtained by sampling the above probability distribution. Note that the most probable patterns are those that globally minimize the Gibbs energy. To obtain these minimum-energy, or "ground state"[3] patterns, we use a Monte Carlo algorithm with simulated annealing, in which the temperature is cooled down according to a schedule slow enough to maintain equilibrium. It is important to remember that the consideration of these patterns is justified by the fact that in MAP estimation, it is imperative to understand the contribution of the *prior* distribution to the structure of the MAP estimate.

In [3], Cross and Jain observed that sampling textures directly from the Gibbs distribution (30) often produces patterns in which one color predominates. To remedy this situation, they proposed that a uniform histogram constraint be imposed on the sampled patterns and that the Metropolis exchange algorithm be used to sample them. The uniform histogram assumption guarantees that all gray levels will be present in the sampled textures. The exchange algorithm operates on an initial random image by moving around pixels in the image to form the texture pattern. In this manner, the histogram of the initial state is preserved throughout the synthesis process. In this paper, we adopt both the uniform histogram assumption and the Metropolis exchange algorithm to sample patterns. An important consequence of imposing the *global* histogram constraint is that the Gibbs distribution (30) no longer induces a *local* Markov random field structure with respect to the neighborhood system for which the clique potentials were defined. This fact has often been overlooked in the literature.

[2] V_{sr} here is defined to be equal to one half times the potential of the two-site clique, {s,r}, of statistical mechanics.

[3] Another expression is "equilibrium state at $T = 0$."

Let us now describe in more detail the sampling algorithm. We start by randomly picking up two sites of different pixel values. The Gibbs energy is computed for the lattice in its current state, E_1, and again in the state with the gray levels at the two sites exchanged, E_2. If we let $\Delta E = E_2 - E_1$ be the energy change, then the sites are exchanged with probability $\min(1, \exp(-\Delta E/T))$. This update probability implicitly forms a ratio of the probabilities of the sites after and before the exchange. This ratio eliminates the need for computing the partition function Z and has the notable side effect of canceling out all terms that appear as constants in the Gibbs energy function. In this paper, as in [3, 22], we assume a constant external field in (29), i.e., the V_s's are independent of the site location s, so that these will cancel in the ratio. Thus, we omit these terms from the Gibbs energy.

When the temperature is nonzero, any pattern in the configuration space has a nonzero probability to be sampled. However, it is important to note that the probabilistic update rule in Metropolis sampling tends to produce lower energy states which are also the most likely states.

Monte Carlo texture synthesis methods produce many different looking states on the way to the ground state. Many of these states look like natural textures. One of the shortcomings of the GRF approach to date is that it has been difficult to predict the evolution of the texture patterns during the equilibrating process. With the aura formulation, we can now better characterize this evolution – both intuitively and numerically.

The aura formulation reinterprets the energy function as an interaction between physical miscibilities. With this intuitive interpretation, one can ask questions such as "are colors A and B maximally separated yet?" The answers to these questions characterize the pattern's progress toward its ground state. Thus, the aura measure is a tool for predicting the appearance and arrival of ground states. This reformulation is now shown. Some examples of its usage will be shown in Section 6.

5.3 New Linear Formulation in Terms of Aura Measures

In this section we show how the GRF can be reformulated using aura measures. The aura allows GRF's to be linked in a straightforward way to both morphological dilation, see Section 2, and to co-occurrence statistics, see Section 4. Most importantly, the new linear aura formulation allows us to better characterize the patterns produced by the GRF. The reader will notice that we pose and analyze our problem in terms of energy minimization. This is for two main reasons. The first is that we are interested in the effect that the prior distribution has during MAP optimization, and the second is that the Metropolis sampling procedure itself tends to favor patterns of low energy.

5.3.1 Isotropic Case

The problem of sampling the most likely textures from a GRF with a uniform histogram constraint can be formulated as the following constrained integer nonlinear programming problem:

$$\begin{aligned} \min_{\mathbf{x}\in\boldsymbol{\Omega}} \quad & \sum_{s\in\mathcal{S}}\sum_{r\in\mathcal{N}_s} V_{sr}(x_s, x_r), \\ \text{subject to} \quad & |\mathcal{S}_g| = \gamma,\ \forall g \in \Lambda = \{0, 1, \ldots, n-1\}, \end{aligned} \tag{31}$$

where the functions V_{sr} represent the pairwise interaction potential between a gray-level value x_s and each of its neighbors $x_r, r \in \mathcal{N}_s$, and $\mathcal{S}_g$ is the set of all gray levels having value g. Notice that the constraints of (31) are not independent because the sum of the sizes of the n gray-level sets, $n\gamma$, must equal $|\mathcal{S}|$. It is important to stress that these constraints are implicitly satisfied when an exchange algorithm such as the Metropolis method is used. Thus, in all the texture synthesis examples of this paper where we start with an initial histogram satisfying $|\mathcal{S}_g| = \gamma$, $\forall g \in \Lambda$, these constraints will also be satisfied by the final pattern. If a non-exchange method were used, histogram constraints would have to be explicitly incorporated into the optimization.

Now, let us consider the case where the image field is homogeneous and isotropic so that the function V_{sr} is independent of both the location of the site, s, and the orientation of its neighbors, $r \in \mathcal{N}_s$. Under this assumption, we write $V_{sr} = V$. Let $m(g,g')$ be the aura measure of the gray-level sets $\mathcal{S}_g$ and $\mathcal{S}'_g$ as defined in Section 3. In this case, we have the following new formulation

Proposition 14 *Let $\{\mathcal{S}_g, g \in \Lambda\}$ be a partition of $\mathcal{S}$ where $x_s = g$ if $s \in \mathcal{S}_g$. Then a nonlinear cost function of the form*

$$\sum_{s \in \mathcal{S}} \sum_{r \in \mathcal{N}_s} V(x_s, x_r), \tag{32}$$

can be rewritten using aura measures as a linear cost function of the form

$$\sum_{g,g' \in \Lambda} V(g,g')m(g,g'). \tag{33}$$

The proof of this proposition is given in Appendix D.

Thus the problem of GRF texture generation in the gray-level domain can be transformed to a linear problem in the "miscibility domain"[4]. Moreover, since each aura measure is nonnegative, if the $V(g,g')$ are all positive (negative), then the original optimization problem reduces to minimizing (maximizing) the individual aura measures.

If a thermodynamic view is considered we can treat the gray levels as pure substances whose self and inner interactions are described by the potential function V. $V(g,g')$ can be considered the *intensive* quantity, independent of the number of particles (pixels) present in the system; it describes the interaction of the pure substances g and g'. The aura measure $m(g,g')$ can be considered the conjugate *extensive* quantity, dependent on the number of particles [27]. The summation (33) then manifests that the pairwise interaction energy between the pure substances is the sum over all interacting pairs of the product of the intensive and extensive quantities describing the interaction of each pair. If we separate the interactions within each substance from the interactions between substances, we can write the optimization problem as

$$\begin{array}{ll} \min\limits_{\mathbf{x} \in \mathbf{\Omega}} & \left(\sum\limits_{g \in \Lambda} V(g,g)m(g,g) + 2 \sum\limits_{g < g'} V(g,g')m(g,g') \right), \\ \text{subject to} & |\mathcal{S}_g| = \gamma, \ \forall g \in \Lambda, \end{array} \tag{34}$$

where we have used the fact that $V(g,g') = V(g',g)$ [5], and that the neighborhood structure is symmetric, which implies that $m(g,g') = m(g',g)$. This form shows that the cost function contains two terms. The first is a weighted sum of the self-aura measures of the gray-level sets. The higher the self-aura measure, the "more clumped" appears the gray-level set. The second term in the cost function is a weighted sum of the "cross-aura" measures of different gray levels – measuring the "mixing" between two different sets. Each weight is equal to the potential of the two gray values. One can already see from (34) that when the $V(g,g')$ are all positive then the measures with large coefficients will be minimized as much as possible. The opposite happens when all the $V(g,g')$ are negative. When the $V(g,g')$ are of different signs, the linearity allows us to divide it into the positive and negative pieces, optimizing each. The latter case will be elaborated in 5.3.2 where we treat the anisotropic case. In the next paragraph, we give two special forms for the isotropic interaction potentials that have found wide use in the GRF texture synthesis literature.

Special Cases We have applied the aura framework to two special cases: the autobinomial model and the Potts model. These two models differ drastically when the number of gray levels is greater than 2. However, when it is equal to two, they both reduce to the Ising model of lattice magnetism.

[4] The reason for using this expression will be explained further in Section 6.

[5] $V(x_s, x_r) = V(x_r, x_s)$, $\forall s \in \mathcal{S}$, $\forall r \in \mathcal{N}_s$, because of the interaction symmetry in a clique.

	4	3	4	
4	2	1	2	4
3	1	s	1	3
4	2	1	2	4
	4	3	4	

(a)

	β_7	β_5	β_8	
β_7	β_3	β_2	β_4	β_8
β_6	β_1	s	β_1	β_6
β_8	β_4	β_2	β_3	β_7
	β_8	β_5	β_7	

(b)

Figure 3: (a) Neighbors of the point s for model orders 1-4. The neighborhood of order p contains all points with labels $\leq p$. (b) The autobinomial parameter for each neighbor.

Before introducing these GRF models, two definitions are needed. The first is the *order* of a neighborhood. In Figure 3 (a) the neighborhoods corresponding to GRF's of orders 1-4 are shown. These are the only orders used in this paper, although extension to higher orders is straightforward. In Figure 3 (b) the autobinomial "bonding parameter" which multiplies each neighbor is shown. The second definition we need is that the autobinomial parameters are isotropic when $\beta_r = \beta$, $\forall r \in \mathcal{N}$. When the model is first order isotropic with $x_s \in \{0, 1\}$, we get a binary nearest-neighbor model from which the famous Ising model [28] can be derived by making the transformation $x_s \to 2x_s - 1$.

The autobinomial model was first introduced in the statistics literature by Besag [1] and first studied as a texture model by Cross and Jain [3]. In the isotropic case, we have $V(g, g') = -\beta g g'$. Letting $\beta = -1$, the miscibility optimization problem is given by

$$\begin{aligned} \min_{\mathbf{x} \in \mathbf{\Omega}} \quad & \left(\sum_{g \in \Lambda} g^2 m(g, g) + 2 \sum_{g < g'} g g' m(g, g') \right), \\ \text{subject to} \quad & |\mathcal{S}_g| = \gamma, \ \forall g \in \Lambda. \end{aligned} \tag{35}$$

When the autobinomial model is synthesized using the Metropolis exchange algorithm it has the property of symmetry with respect to the gray-level values. That is, if each gray level $g \in \Lambda = \{0, 1, \ldots, n-1\}$, is replaced with a new gray level according to $g \to n - 1 - g$, then the parameters of the synthesized pattern do not change. This property is useful in simulations when we analyze the patterns formed.

The second special case we consider is the Potts model from statistical mechanics [29]. It was used by Geman and Geman [5] in the context of image restoration and by Derin and Elliott [25] in the context of texture-based image segmentation. In these references the external field was assumed zero (i.e., no single-site clique potentials). Also, the Gibbs sampler (non-exchange) method was used to generate texture patterns, and no constraint was imposed on the image histogram. The pairwise interaction energy for the Potts model can be written, within a scaling constant that we will assume positive, as $V(g, g') = 2\delta_{gg'} - 1$ where $\delta_{gg'}$ is the Kronecker δ symbol. In this case, the miscibility optimization problem becomes

$$\begin{aligned} \min_{\mathbf{x} \in \mathbf{\Omega}} \quad & \left(\sum_{g \in \Lambda} m(g, g) - 2 \sum_{g < g'} m(g, g') \right), \\ \text{subject to} \quad & |\mathcal{S}_g| = \gamma, \ \forall g \in \Lambda. \end{aligned} \tag{36}$$

The famous Ising model, mentioned in connection with the boundary length principle in Section 3, is a special case of both the autobinomial and Potts models. Let S_1 be the set of sites with spin up, and S_{-1} be the set of sites with spin down. The most likely patterns of the isotropic Ising model are the solutions the optimization problem

$$\min_{\mathbf{x}\in\mathbf{\Omega}}(-\beta)[m(S_{-1}, S_{-1}) + m(S_1, S_1) - 2m(S_1, S_{-1})].$$

Note that we have omitted the histogram constraint for this example. When $\beta > 0$, the expression between brackets is maximized. The maximum occurs when either every site is 1 or every site is -1 so that $m(S_{-1}, S_1) = 0$ (spontaneous magnetization). Without the histogram constraint, the minimum boundary length is zero. When $\beta < 0$, the expression is minimized. This corresponds to the antiferromagnetic phase.

In general the energy optimization problem can be recast as a boundary optimization problem. When the uniform histogram constraint is imposed this problem becomes one of constrained boundary optimization, see Paragraph 5.3.3 below. For the Ising model on a lattice of known size, if we know the total number of up spins $|S_1|$ and the total number of pairs of up spins $m(S_1, S_1)$, the model is completely characterized. This characterization in terms of boundary length is well known in the physics literature [28]. Here we have shown that it is a special case of the new aura matrix properties. Thus, we have a new boundary length characterization for any number of gray levels, not just for the binary Ising model.

5.3.2 Anisotropic Case

The objective of this section is to extend the linear formulation to accommodate the important case where the field is anisotropic. We assume that the neighborhood of each site, $\mathcal{N}_s$, can be partitioned into K subneighborhoods, $\mathcal{N}_s^k$, so that in each subneighborhood the field behaves isotropically. From Section 3 we have the two equalities,

$$\mathcal{N}_s = \bigcup_{k=1}^{K} \mathcal{N}_s^k, \quad \forall s \in \mathcal{S}, \tag{37}$$

where $\mathcal{N}_s^k \cap \mathcal{N}_s^l = \emptyset, \ \forall l \neq k$, and

$$m(g, g') = \sum_{k=1}^{K} m^k(\mathcal{S}_g, \mathcal{S}_{g'}), \tag{38}$$

so that the aura measures are a sum of co-occurrences.

Proposition 15 *Let $\{\mathcal{S}_g, g \in \Lambda\}$ be a partition of $\mathcal{S}$ where $x_s = g$ if $s \in \mathcal{S}_g$. Let the symmetric neighborhood $\mathcal{N}$ be partitioned into K isotropic subneighborhoods. Then the anisotropic nonlinear cost function,*

$$\sum_{s\in\mathcal{S}} \sum_{r\in\mathcal{N}_s} V_r(x_s, x_r), \tag{39}$$

can be rewritten using aura measures as a linear cost function in the form

$$\sum_{k=1}^{K} \sum_{g,g'\in\Lambda} V^k(g, g')m^k(g, g'). \tag{40}$$

The proof of this proposition is given in Appendix E.

Thus, for the anisotropic case, we obtain a linear combination of isotropic aura measures on subneighborhoods. Because of linearity, miscibility analysis developed for the isotropic case can be directly extended to the anisotropic case. Also, intuition developed about mixing and about boundary minimization is easily extended to the anisotropic case via superposition.

Special Cases As before, we consider the autobinomial and Potts models. Using Proposition 15, the anisotropic autobinomial function to be maximized is

$$\sum_{k=1}^{K} \beta_k \sum_{g,g' \in \Lambda} g g' m^k(g,g'). \tag{41}$$

We see that it is just a linear combination of K isotropic cases, with weights equal to the bonding parameters.

Similarly, the Potts model becomes

$$\sum_{k=1}^{K} \beta_k \sum_{g,g' \in \Lambda} (2\delta_{gg'} - 1) m^k(g,g'). \tag{42}$$

It is important at this stage to mention the work of Cross [2]. Cross calculated co-occurrences for the special case of the binary first-order GRF (i.e., Ising model) on an $N \times N$ lattice with toroidal boundary, zero external field, and uniform histogram. Using an approximate analytical expression for the Z partition function that is valid for large lattice sizes, Cross gave analytical expressions for the expected values of the co-occurrences. This allowed him to determine how these expected co-occurrences depend on the parameters of the first-order GRF model. He also verified this dependence using Monte Carlo simulations of an isotropic, first-order binary GRF model.

Note that there does not exist such an expression for Z in the general gray-level autobinomial model, and hence Cross's results do not extend to more than two gray levels. However, the aura measure formulation of the Gibbs model forms an explicit connection between co-occurrences and the general autobinomial GRF. By writing the Gibbs energy (with the assumed pairwise cliques) as a linear combination of co-occurrences, we have shown that the co-occurrences are a sufficient statistic. Thus, the autobinomial Gibbs distribution can be considered an implicit model when co-occurrence based analysis is conducted.

5.3.3 Constraints on Aura Measures

From an optimization point of view, the most interesting fact about expressing the cost function in terms of the aura measures is that it becomes linear as a function of these variables. We can go one step further along the way of transforming the nonlinear integer program into a linear integer program by introducing linear constraints on the aura measures. These linear constraints are of two kinds: equality constraints due to the uniform histogram assumption and inequality constraints imposed by the lattice geometry and boundary conditions.

The first kind of constraints can be readily obtained from the aura matrix properties given in Proposition 11. Specifically, the aura measures satisfy $n = |\Lambda|$ equality constraints given by

$$\sum_{g' \in \Lambda} m(g,g') = |\mathcal{S}_g||\mathcal{N}|, \; \forall g \in \Lambda. \tag{43}$$

The inequality constraints are more difficult to obtain because they strongly depend on the particular texture synthesis problem we are dealing with.

To give a flavor of these inequality constraints, consider again the binary ferromagnetic Ising model with uniform histogram and periodic boundary conditions. Define the gray-level sets $\mathcal{S}_0$ and $\mathcal{S}_1$ to be the sets of 0's and 1's respectively. The cost function to be minimized is reduced to $-m(1,1)$, under the equality constraints

$$\begin{aligned} m(0,0) + m(0,1) &= 2|\mathcal{S}|, \\ m(0,1) + m(1,1) &= 2|\mathcal{S}|. \end{aligned}$$

Minimizing the cost function means (intuitively) maximizing the "clumpiness" of the white pixels. From the two equality constraints, this implies that $m(0,1)$ will be minimized, and $m(0,0)$ consequently maximized. It is clear that the simultaneous presence of both black and white pixels imposes a lower bound on $m(0,1)$. This lower bound depends on the geometry of the lattice; it is the inequality constraint we need.

For a square periodic lattice with $|\mathcal{S}| = N^2$, the lower bound on $m(0,1)$ is $2N$ and is reached by a configuration in which the black and white pixels form two adjacent stripes. An alternate configuration, where one color forms a circular clump surrounded by the other color, does not give as short of a boundary as does the striped configuration. With equal numbers of black and white, the circular boundary has length approximated by $\sqrt{2\pi}N$, which is greater than $2N$.

For the binary case with a rectangular $M \times N$ lattice, the two stripes will be parallel to the smaller of the rectangle dimensions so that the inequality constraint is $m(0,1) \geq 2\min(M,N)$. Note that this is an example where even with isotropic parameters, the ground state will not be isotropic. This new boundary length formulation of the GRF enables us to intuit many cases where lattice geometry influences ground state configurations.

For higher numbers of gray levels, one can follow a similar approach of partitioning the lattice into regions approximating circles and stripes. For the autobinomial model on a square lattice, when self-measures are being maximized, gray levels 0 and $n-1$ will form circles separated by gray levels $1, \ldots, n-2$ which form stripes. In some cases, the energy of the "all stripes" configuration is very close to the energy of the "circles and stripes" configuration, so that samples of both types of configurations are readily formed.

A somewhat inverted analysis holds for the minimum self-miscibility case of the autobinomial energy, where stripes are formed of mixtures of gray levels, and the color that forms a clump (when n is odd) is the middle color, $(n-1)/2$. The reader is referred to Section 6 for examples of autobinomial near-minimum energy patterns on square and non-square lattices.

6 Simulations

Now we apply the aura measures to the analysis of synthesized GRF texture patterns. This will enable us to characterize what the patterns will look like near their minimum energy states. The simulations here assume a rectangular $M \times N$ lattice with periodic boundary conditions and the autobinomial GRF energy function described in Section 5.3.1.

The samples have been synthesized by the Metropolis exchange method, with log annealing according to the schedule

$$T = \frac{c}{\log(\lfloor i/10 \rfloor + 1)},$$

where $i = 0, 1, \ldots$ is the iteration number. The scale factor in the numerator is typically chosen in the range $c \in (0, 10]$. Although its choice is ad hoc (theoretically optimal choices are impractical, see Geman and Geman [5]), its behavior is understood as a rate constant that is proportional to how slow the annealing progresses. One iteration is counted as MN attempted exchanges. An exchange is attempted whenever two randomly picked sites have different locations and gray levels. The total number of iterations for the patterns was 10000, with the temperature lowered according to the above schedule every 10 iterations. The initial state for all these simulations was a random noise image with uniform histogram. Because of the exchange operation in the Metropolis algorithm, the histogram is preserved throughout the texture synthesis and the (assumed constant) external field can be ignored.

6.1 Mixing and Separation

For isotropic parameters the behavior of the autobinomial GRF is easily described by its gray-level miscibilities, or "mixing". In Section 4.4 we defined the miscibility measures to be the aura measures, normalized by the product of the uniform histogram height and neighborhood size. The normalized

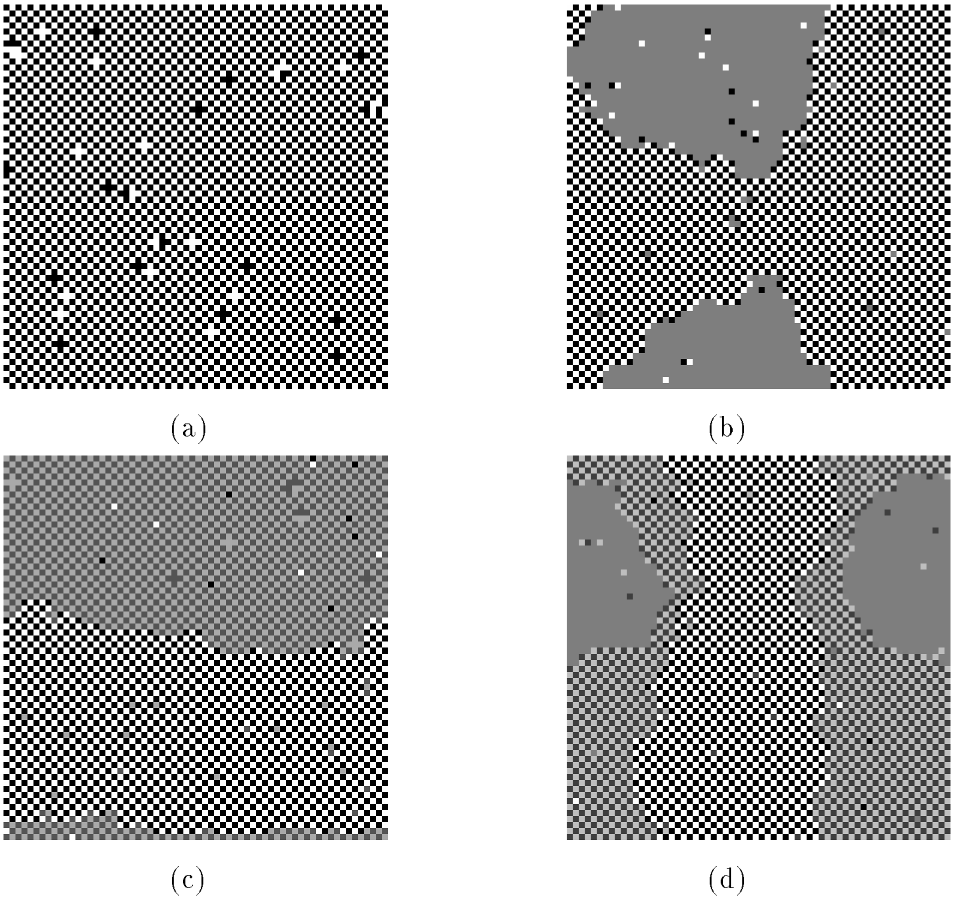

Figure 4: Examples of near-minimum-energy patterns for first-order autobinomial GRF with negative isotropic bonding parameters. Images (a)-(d) correspond to 2-5 gray levels respectively. Each image is 64×64.

---

case is important when the aura matrix is to be analyzed probabilistically. However, the distinction is quantitative, not qualitative. For forming intuition about the GRF synthesis, the "miscibility" and "aura measure" behavior are the same.

In Figure 4 are shown four texture samples corresponding to first-order negative isotropic parameters. All of these have identical parameters; the only difference is that the number of gray levels in (a)-(d) changes from 2 to 5. These patterns are close enough to their ground states that the minimum energy characteristics are easily seen. The reader is referred to Expression (35) for notation and problem formulation.

In (a) we see the checkerboard being made in an effort to minimize $m(1,1)$ (white self-miscibility). The terms $m(0,0)$ and $m(0,1)$ are multiplied by zero and can be ignored. Optimization is achieved by moving blacks between all the whites, so that the miscibility of the whites goes to zero. In (b) the sum of $m(1,1)$, $4m(2,2)$, and $4m(1,2)$ is minimized. The last two terms have the greatest weight, and can be interpreted as color 2 (white) trying to form a mixture, but not with itself or color 1 (gray). This leaves the configuration of a checkerboard between colors 0 (black) and 2, with color 1 forming a clump off by itself. The behavior of this case and other cases where one color does not mix with any other is perhaps captured in the witticism, "if you're not part of the solution, then you're part of the precipitate." To minimize the term $m(1,1)$ it would be necessary to have a fourth color to mix with it. This happens in (c). The image in (d) and images made with higher numbers of gray levels have similar explanations, all deriving from intuition about mixing.

For positive isotropic parameters the behavior is described by immiscibility, the separation of the different colors (or "fluids"). Figure 5 is identical to that of Figure 4 with the exception of the sign of β. In (a) the black and white separate as $m(1,1)$ is maximized. If the synthesis of this energy function

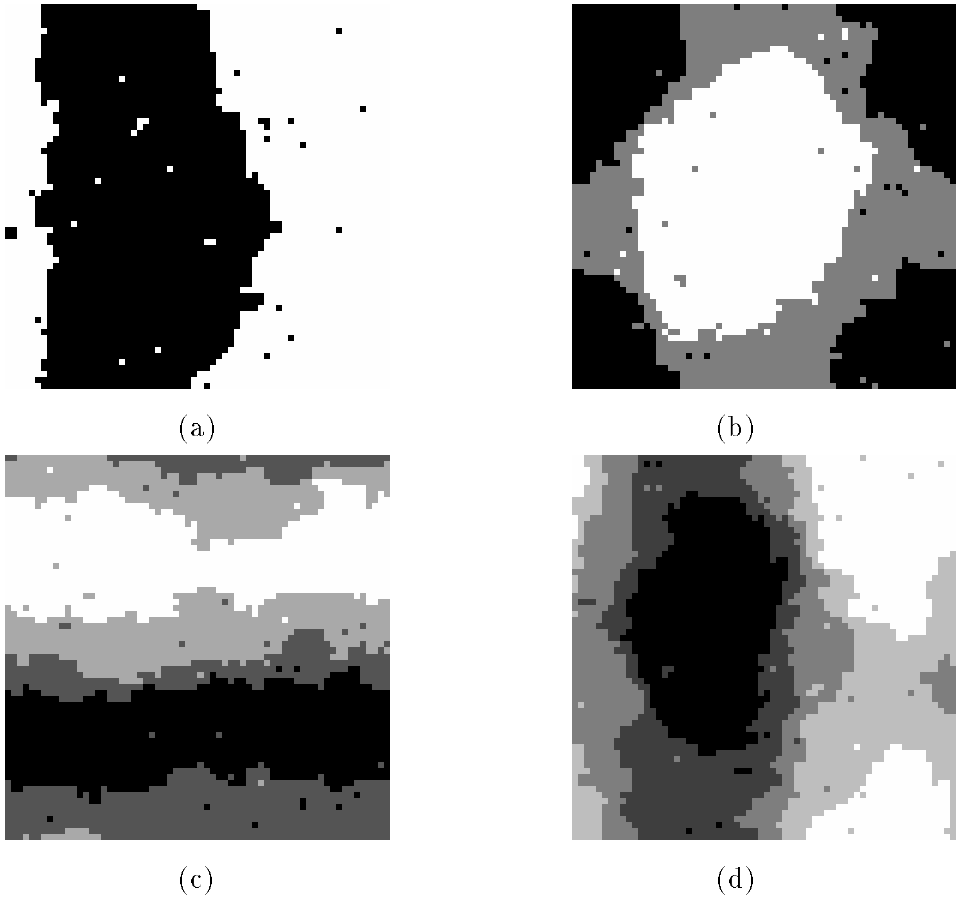

Figure 5: Examples of near-minimum-energy patterns for first-order autobinomial GRF with positive isotropic bonding parameters. Images (a)-(d) correspond to 2-5 gray levels respectively. Each image is 64×64.

---

were done using a non-exchange method such as the Gibbs Sampler, the optimal pattern would be solid white. The black remains only because of the exchange method which preserves the histogram of the lattice. In (b) the sum of $m(1,1)$, $4m(2,2)$, and $4m(1,2)$ is maximized. Gray level 2 forms a clump while maximizing the presence of gray level 1 along its boundary. Gray level 0 is left with no choice but to form a clump. The image in (c) and images made with higher numbers of gray levels have similar explanations which derive from intuition about separation.

As mentioned before, for autobinomial fields synthesized with the Metropolis exchange, the result should be the same if all the gray levels of value g are replaced with those of value $n - g - 1$. This gray level symmetry is seen in the miscibility behavior. For example, both black (0) and white $(n - 1)$ have the same mixing behavior in all the samples shown in this section.

6.2 Boundary Maximization and Minimization

The mixing and separation described in the previous section has another interpretation in terms of gray level boundary length. The behavior that was described for the Ising model in Section 5.3.1 is an example of the boundary length optimization for the binary case. The examples in Figure 4 are, however, examples of maximizing gray level boundary length for a general number of gray levels. Similarly, Figure 5 gives examples of minimizing gray level boundary length.

When the lattice geometry is not square, the boundary minimization can manifest itself differently. As mentioned in Section 5.3.3 there is a geometry-dependent lower bound for the cross-miscibility measures. Of all the configurations that separate white and black, the one they will choose will be the one with minimum total boundary length. On a 32×64 lattice, this is a left-right separation,

(a) (b)

Figure 6: Lattice geometry affects the equilibrium pattern by constraining the miscibilities between different gray levels. In (a), the separation makes a vertical boundary since that dimension is shortest in this 32×64 lattice. Note this pattern is only two exchanges from being at its minimum energy state. Similarly, in (b), the two gray regions try to separate with vertical boundaries.

---

with boundary length proportional to 2×32. (There are two boundaries since the lattice is periodic). An example of this selection is illustrated in Figure 6 for gray levels 2 and 3. The parameters used to synthesize these patterns are identical to those used in Figure 5 (a) and (b), but the model order has been increased to four. The higher order neighborhood yields the less noisy appearance of these patterns.

6.3 Aura Matrices and Isotropic Texture Samples

Boundary length and miscibility are numerically represented in the aura matrices. Aura matrices for the texture samples of Figure 4 (a)-(d) are shown in Figure 7. Note that the auras were all formed with first order neighborhoods ($|\mathcal{N}| = 4$), as the texture samples are all first order GRF's. The aura matrix properties are easily checked for the $|\mathcal{S}| = 64 \times 64$ lattices used here. We note that all of the aura matrices are becoming anti-tridiagonal. For the positive bonding parameters, they become tridiagonal. In another paper [30], the authors establish more precisely the conditions under which this behavior occurs. The tridiagonal aura matrices are shown in Figure 8. The diagonal dominance of co-occurrence matrices has long been understood to relate to pattern "clumpiness" [16]. Here the aura self-measures give a quantitative measure of this patterning.

From the aura-based analysis and simulations, it appears that the patterns generated by Cross and Jain [3] which they said had "converged" much sooner than these, were not actually near their minimum energy states. Instead, they were still changing, albeit slowly, and approaching patterns such as we have shown. How far a given pattern is from its ground state is still an interesting question. We have begun investigating the ability of the aura to represent this "distance" by examining its trace during the energy minimization. The trace can be shown to grow linearly with the number of gray levels [30]. For higher order neighborhoods the matrices tend to become tridiagonal faster, resulting in a steeper slope of the trace vs. the number of gray levels. For negative parameters, the *anti-trace*, which is the sum of matrix elements along the *anti-diagonal* linking the matrix upper right and lower left corners, plays a role similar to that of the trace in the positive parameter case.

Other features of the aura matrix such as entropy, correlation, and bandwidth have also been shown to characterize behaviors of the autobinomial texture, such as sudden changes which are analogous to

$$\mathbf{A} = \begin{bmatrix} 138 & 8054 \\ 8054 & 138 \end{bmatrix}$$

(a)

$$\mathbf{A} = \begin{bmatrix} 0 & 170 & 5290 \\ 170 & 5116 & 174 \\ 5290 & 174 & 0 \end{bmatrix}$$

(b)

$$\mathbf{A} = \begin{bmatrix} 0 & 0 & 159 & 3937 \\ 0 & 34 & 3903 & 159 \\ 159 & 3903 & 34 & 0 \\ 3937 & 159 & 0 & 0 \end{bmatrix}$$

(c)

$$\mathbf{A} = \begin{bmatrix} 0 & 0 & 0 & 140 & 3136 \\ 0 & 0 & 100 & 3032 & 144 \\ 0 & 100 & 3072 & 104 & 0 \\ 140 & 3032 & 104 & 0 & 0 \\ 3136 & 144 & 0 & 0 & 0 \end{bmatrix}$$

(d)

Figure 7: Aura matrices corresponding to textures in Figure 4 (a) – (d).

$$\mathbf{A} = \begin{bmatrix} 7878 & 314 \\ 314 & 7878 \end{bmatrix}$$

(a)

$$\mathbf{A} = \begin{bmatrix} 5174 & 286 & 0 \\ 286 & 4904 & 270 \\ 0 & 270 & 5194 \end{bmatrix}$$

(b)

$$\mathbf{A} = \begin{bmatrix} 3850 & 246 & 0 & 0 \\ 246 & 3598 & 252 & 0 \\ 0 & 252 & 3594 & 250 \\ 0 & 0 & 250 & 3846 \end{bmatrix}$$

(c)

$$\mathbf{A} = \begin{bmatrix} 3072 & 204 & 0 & 0 & 0 \\ 204 & 2828 & 244 & 0 & 0 \\ 0 & 244 & 2794 & 238 & 0 \\ 0 & 0 & 238 & 2836 & 202 \\ 0 & 0 & 0 & 202 & 3078 \end{bmatrix}$$

(d)

Figure 8: Aura matrices corresponding to textures in Figure 5 (a) – (d).

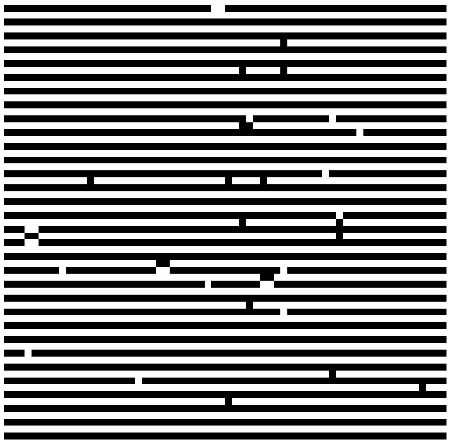

$$\mathbf{A_{11}} = \begin{bmatrix} 4030 & 66 \\ 66 & 4030 \end{bmatrix}$$

$$\mathbf{A_{12}} = \begin{bmatrix} 64 & 4032 \\ 4032 & 64 \end{bmatrix}$$

$$\mathbf{A} = \begin{bmatrix} 4094 & 4098 \\ 4098 & 4094 \end{bmatrix}$$

Figure 9: The pattern on the left was synthesized using a binary GRF with $\beta_{11} = 1$ (horizontal) and $\beta_{12} = -1$ (vertical). The aura matrices for these two isotropic neighborhoods are shown to illustrate that their sum gives the anisotropic aura matrix.

---

phase transitions [31].

6.4 Anisotropic Fields

With the linear formulation of (40) we know that the aura matrices of anisotropic texture patterns will be a sum of the tridiagonal and anti-tridiagonal matrices taken over isotropic subneighborhoods. An example of the superposition of aura matrices in the anisotropic case is shown in Figure 9. Here, the magnitudes of the bonding parameters are equal, $|\beta_k| = 1$, and the aura matrices over the two subneighborhoods are nearly the reflection of each other. Their sum gives the aura matrix over the anisotropic neighborhood, $\mathcal{N}$.

An important consequence of this linearity is that it reveals constraints on the types of structure that can appear in co-occurrence matrices of these textures, and in turn, on the patterns which can exist in *a priori* images modeled by the ground states of the GRF. For example, for $n = 5$, $m(0, 2) = m(2, 0)$ and $m(2, 4) = m(4, 2)$ may be forced to be zero in the ground state. This means that certain gray levels can not occur as neighbors in the ground state textures produced by the model! This can be a serious limitation of this model; it is addressed specifically elsewhere [30].

Now we consider anisotropy with β_k of varying magnitude. As the relative magnitudes of the parameters are changed, the relative weights of the miscibilities change as given in (40). In Figure 10, the parameters are $\beta_1 = 1$ (horizontal), $\beta_2 = 1$ (vertical) on the left and $\beta_1 = 1$, $\beta_2 = 2$ on the right. The stronger vertical clustering is apparent on the right. Similarly, Figure 11 has parameters $\beta_1 = -1$, $\beta_2 = -1$ on the left, and $\beta_1 = -1$, $\beta_2 = -2$ on the right. Here, the vertical tug is evident from the vertical crystal defects. These result because the repulsion between vertical pairs is stronger than the repulsion between horizontal pairs. An alternate interpretation of this behavior is that the rate of optimization in the vertical direction is twice that in the horizontal direction [32]. Either way, the aura matrix gives both a quantitative and more intuitive characterization of the texture pattern throughout its formation.

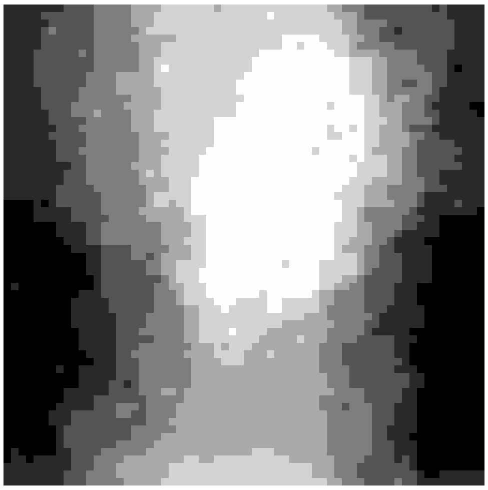

(a)

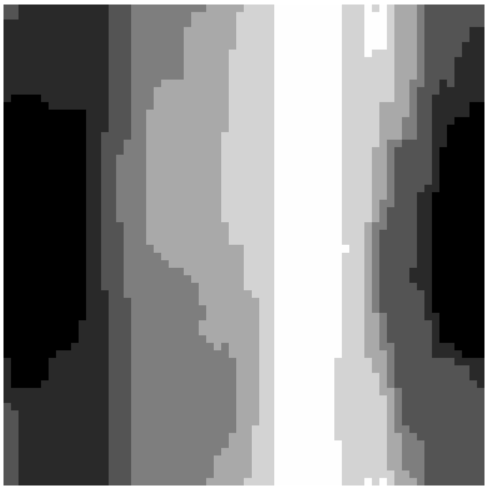

(b)

Figure 10: Comparison of isotropic (a) and anisotropic (b) positive parameters. The vertical parameter in (b) has twice the value of the horizontal parameter. Both images have 7 gray levels and are 64×64.

---

7 Conclusions

We have introduced a new set-theoretic neighborhood-based framework and shown its application to Gibbs texture modeling. The framework has also been applied to establishing relationships between the GRF, co-occurrences, and morphological dilation. The basic tools are the "aura set" which describes the relative presence of a set A in the neighborhood of another set B, and the measure of this set, the "aura measure." The latter provides a generalization of co-occurrence statistics to any neighborhood system and any sampling lattice. Moreover, the aura measure yields a new interpretation of co-occurrences as gray-level set boundaries that can be related to physical intuition about the mixing and separation of multiphase fluids.

When the aura measures are considered together for all gray levels, they define an "aura matrix" that generalizes the co-occurrence matrix. We have described how various histogram and lattice assumptions introduce constraints on the coefficients of the aura matrix and hence also on those of the co-occurrence matrix. It has also been discussed how the aura formulation of the GRF assists one in predicting the more probable (lower energy) patterns of the Gibbs model. The results obtained in this paper allow us to make the following conclusions:

(a) The nonlinear Gibbs energy can be rewritten as a linear combination of co-occurrence measures over the Markov neighborhood.

(b) The linear form of the Gibbs energy allows the texture patterns to be both mathematically and intuitively characterized by the amount of mixing and separation between gray levels.

(c) The aura measure formulation of the Gibbs energy, which holds for any number of gray levels or neighborhood order, generalizes the "boundary length optimization" property of the (binary, first-order) Ising model.

(d) During the synthesis of texture the lattice geometry and Metropolis exchange algorithm enforce constraints on the matrix of aura measures, and hence on the co-occurrences. These constraints suggest that the co-occurrences may be a useful tool for measuring distance of the GRF from its minimum energy configuration.

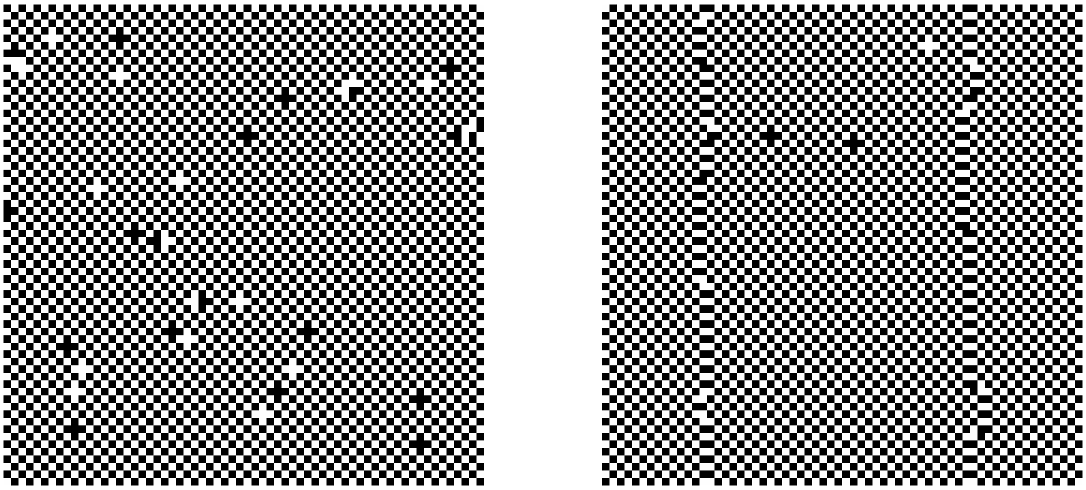

(a) (b)

Figure 11: Comparison of isotropic (a) and anisotropic (b) negative parameters. The vertical parameter in (b) has twice the value of the horizontal parameter so its defects favor vertical repulsion. Both images have 2 gray levels and are 64×64.

(e) Though the GRF as studied here is a local interaction model, a linear combination of co-occurrence matrices over the GRF neighborhood also contains information about global interactions between gray-level sets. These global interactions result in a large scale structure that is not obvious from the GRF bonding parameters alone.

Even though we are still in the process of exploring the set theoretic framework for texture analysis and prediction, we feel that the work presented in this paper has already confirmed Besag's observation that we quote from his seminal paper [1]:

> *Incidentally, the fact that a scheme is formally described as "locally interactive" does not imply that the patterns it produces are local in nature (cf. the extreme case of long-range order in the Ising model).*

8 Acknowledgments

The authors acknowledge the helpful support and encouragement of John Wyatt, Jr. and Alex P. Pentland. Thanks to Pentland for suggesting a connection between the aura and morphological dilation and to Roland R. Netz for fun and helpful discussions about Gibbs equilibrium. We are indebted to a number of anonymous colleagues, as well as to Kris Popat and Fang Liu for providing helpful comments on earlier drafts of this paper.

The work described in this paper was supported by the National Science Foundation and the Defense Advanced Research Projects Agency (DARPA) under Grant No. MIP-88-14612, the National Science Foundation under Grant No. IRI-8719920, the Rome Air Development Center (RADC) of the Air Force System Command and the Defense Advanced Research Projects Agency (DARPA) under contract No. F30602-89-C-0022.

A Properties of the aura set and aura measure

Proposition 16 *(Aura Properties) Let $A, B, C \subseteq \mathcal{S}$ with a given neighborhood structure. Then*

(a) The aura of any set with respect to the empty set is empty, i.e.,

$$\mathcal{O}_{\emptyset}(A) = \emptyset, \; \forall A \subseteq \mathcal{S};$$

(b) The aura of A with respect to B is included in B, i.e.,

$$\mathcal{O}_B(A) \subseteq B;$$

(c) The self-aura of A is included in A, i.e.,

$$\mathcal{O}_A(A) \subseteq A.$$

In general, $A \not\subseteq \mathcal{O}_A(A)$, unless the neighborhood structure is defined such that every site of the lattice is in its own neighborhood;

(d) The aura of $A \cup B$ with respect to C is equal to the union of their respective auras with respect to C, i.e.,

$$\mathcal{O}_C(A \cup B) = \mathcal{O}_C(A) \cup \mathcal{O}_C(B);$$

(e) We also have

$$\mathcal{O}_C(A \cap B) \subseteq \mathcal{O}_C(A) \cap \mathcal{O}_C(B).$$

Unlike the union case, the equality is, in general, not satisfied;

(f) If $A \subseteq B$ then

$$\mathcal{O}_C(A) \subseteq \mathcal{O}_C(B);$$

(g) The aura of A with respect to $B \cup C$ is the union of the auras of A with respect to B and C, i.e.,

$$\mathcal{O}_{B \cup C}(A) = \mathcal{O}_B(A) \cup \mathcal{O}_C(A);$$

(h) Similarly,

$$\mathcal{O}_{B \cap C}(A) = \mathcal{O}_B(A) \cap \mathcal{O}_C(A);$$

(i) The aura "operation" is not generally symmetric, i.e.,

$$\mathcal{O}_B(A) \neq \mathcal{O}_A(B).$$

The proofs of these follow from Definition 1 and elementary set operations.

Proposition 17 *(Aura Measure Properties) For a lattice $\mathcal{S}$ with a given neighborhood structure and a given set $B \subseteq S$, then*

(a) $m(., B)$ is a nonnegative function, i.e.,

$$\forall A \subseteq \mathcal{S}, m(A, B) \geq 0;$$

(b) $m(., B)$ is monotonic, i.e.,

$$A \subseteq A' \rightarrow m(A, B) \leq m(A', B);$$

(c) $m(., B)$ is subadditive, i.e.,

$$m(\cup_{i=1}^n A_i, B) \leq \sum_{i=1}^n m(A_i, B).$$

The proofs of these properties follow from Definition 5.

B Proof of Proposition 9

Proof: i $\rightarrow$ ii. By definition, we have

$$\begin{aligned} m(A,B) &= \sum_{s\in A} |\mathcal{N}_s \cap B| \\ m(B,A) &= \sum_{s\in B} |\mathcal{N}_s \cap A|. \end{aligned}$$

We proceed by induction on the number of elements, $|B|$, of the set B. First, let us prove that (8) is satisfied when $|B| = 1$. Denote by b the only element in B. Then $m(B,A) = |\mathcal{N}_b \cap A|$. On the other hand,

$$m(A,B) = \sum_{s\in A} |\mathcal{N}_s \cap \{b\}|. \tag{44}$$

This summation contains either zeros or ones, with ones occurring only when $b \in \mathcal{N}_s$, or by the symmetry assumption, $s \in \mathcal{N}_b$. It follows that

$$m(A,B) = \sum_{s\in \mathcal{N}_b \cap A} 1 = |\mathcal{N}_b \cap A| = m(B,A), \tag{45}$$

which proves (8) for $|B| = 1$. Assume now that (8) is satisfied for all sets B such that $|B| = k \in \{1, \ldots, n-1\}$ and consider a set B such that $|B| = n$. Choosing an element $b \in B$, we can write $B = C \cup \{b\}$ where $C = B - \{b\}$ and $|C| = n - 1$. Now

$$\begin{aligned} m(A,B) &= m(A, C\cup\{b\}) \\ &= \sum_{s\in A} |\mathcal{N}_s \cap (C \cup \{b\})| \\ &= \sum_{s\in A} |(\mathcal{N}_s \cap C) \cup (\mathcal{N}_s \cap \{b\})| \\ &= \sum_{s\in A} (|\mathcal{N}_s \cap C| + |\mathcal{N}_s \cap \{b\}|) \quad \text{(because } C \cap \{b\} = \emptyset) \\ &= \sum_{s\in C} |\mathcal{N}_s \cap A| + |\mathcal{N}_b \cap A| \quad \text{(by the induction assumption)} \\ &= \sum_{s\in C\cup\{b\}} |\mathcal{N}_s \cap A| \\ &= \sum_{s\in B} |\mathcal{N}_s \cap A| \\ &= m(B,A). \end{aligned} \tag{46}$$

ii $\rightarrow$ i. Let s and r be two pixels such that $r \in \mathcal{N}_s$. We want to prove that $s \in \mathcal{N}_r$. Apply Condition ii to $A = \{s\}$ and $B = \{r\}$. Then we have

$$m(A,B) = |\mathcal{N}_s \cap \{r\}| = |\mathcal{N}_r \cap \{s\}| = m(B,A).$$

It follows that

$$|\mathcal{N}_r \cap \{s\}| = 1,$$

which implies that $s \in \mathcal{N}_r$. ∎

C Proof of Proposition 11

Proof: For (0a) we have

$$\begin{aligned}\sum_{j=0}^{n-1} a_{ij} &= \sum_{j=0}^{n-1} m(S_i, S_j) \\ &= m(S_i, \cup_{j=0}^{n-1} S_j) \\ &= m(S_i, \mathcal{S}) \\ &= |S_i||\mathcal{N}|,\end{aligned}$$

and similarly for (0b). Note that (0a) and (0b) generalize Proposition 19. The proof of (0c) comes directly from Proposition 9 together with (0a) and (0b). ■

D Proof of Proposition 14

Proof: Using the assumptions, we can rewrite (32) as

$$\sum_{g\in\Lambda} \sum_{s\in\mathcal{S}_g} \sum_{r\in\mathcal{N}_s} V(g, x_r). \tag{47}$$

Furthermore,

$$\mathcal{N}_s = \bigcup_{g'\in\Lambda} (\mathcal{N}_s \cap \mathcal{S}_{g'}),$$

and $x_r = g'$ when $r \in \mathcal{S}_{g'}$. It follows that (47) can be written as

$$\sum_{g\in\Lambda} \sum_{s\in\mathcal{S}_g} \sum_{g'\in\Lambda} \sum_{r\in\mathcal{N}_s\cap\mathcal{S}_{g'}} V(g, g'), \tag{48}$$

or

$$\sum_{g,g'\in\Lambda} V(g, g') \sum_{s\in\mathcal{S}_g} |\mathcal{N}_s \cap \mathcal{S}_{g'}|. \tag{49}$$

Using the definition of the measure of an aura for gray-level sets, we get finally

$$\sum_{g,g'\in\Lambda} V(g, g') m(g, g'). \tag{50}$$

■

E Proof of Proposition 15

Proof: Using the assumption that $\mathcal{S}_g$ partitions $\mathcal{S}$ we can rewrite (39) as

$$\sum_{g\in\Lambda} \sum_{s\in\mathcal{S}_g} \sum_{r\in\mathcal{N}_s} V_r(g, x_r). \tag{51}$$

Let $V^k(g, x_r)$ be the value of $V_r(g, x_r)$ in subneighborhood k where the interaction $V_r(x_s, x_r)$ is assumed to be isotropic. Then we obtain

$$\sum_{g\in\Lambda} \sum_{s\in\mathcal{S}_g} \sum_{k=1}^{K} \sum_{r\in\mathcal{N}_s^k} V^k(g, x_r). \tag{52}$$

Now we partition $\mathcal{N}_s^k$ into its different gray levels. When $r \in \mathcal{S}_{g'}$, we have $x_r = g'$, giving,

$$\sum_{g\in\Lambda} \sum_{s\in\mathcal{S}_g} \sum_{k=1}^{K} \sum_{g'\in\Lambda} \sum_{r\in\mathcal{N}_s^k\cap\mathcal{S}_{g'}} V^k(g,g'), \tag{53}$$

which after rearranging, becomes

$$\sum_{k=1}^{K} \sum_{g,g'\in\Lambda} \sum_{s\in\mathcal{S}_g} \sum_{r\in\mathcal{N}_s^k\cap\mathcal{S}_{g'}} V^k(g,g'). \tag{54}$$

This is equivalent to

$$\sum_{k=1}^{K} \sum_{g,g'\in\Lambda} V^k(g,g') \sum_{s\in\mathcal{S}_g} |\mathcal{N}_s^k \cap \mathcal{S}_{g'}|, \tag{55}$$

which gives, finally,

$$\sum_{k=1}^{K} \sum_{g,g'\in\Lambda} V^k(g,g') m^k(g,g'). \tag{56}$$

■

F Aura Measures and Exchange Operations

In this appendix we study how the exchange operation affects the aura measures of the lattice subsets involved in these exchanges.

Let A, B, C be three mutually disjoint subsets of $\mathcal{S}$. Let $A_s \subseteq A$, $B_s \subseteq B$, and $|A_s| = |B_s|$. Assume that the sets A and B have exchanged the two subsets A_s and B_s, so that after the exchange, the sets A and B have become $A' = (A - A_s) \cup B_s$ and $B' = (B - B_s) \cup A_s$, respectively. Our objective is to compare $m(A', A')$, $m(B', B')$, $m(A', B')$, $m(B', A')$ with $m(A, A)$, $m(B, B)$, $m(A, B)$, $m(B, A)$, and to compare $m(A', C)$, $m(B', C)$ with $m(A, C)$, $m(B, C)$. We have the following result:

Proposition 18 *Let A, B, C be three mutually disjoint subsets of $\mathcal{S}$, and let $A_s \subseteq A$, $B_s \subseteq B$. Let also $A' = (A - A_s) \cup B_s$ and $B' = (B - B_s) \cup A_s$. Then,*

$$\begin{aligned} & m(A', A') + m(B', B') + m(A', B') + m(B', A') \\ & \quad = m(A, A) + m(B, B) + m(A, B) + m(B, A), \quad \textit{and} \end{aligned} \tag{57}$$

$$m(A', C) + m(B', C) = m(A, C) + m(B, C). \tag{58}$$

Proof: The basic observation for proving this proposition is that when the two disjoint subsets A, B exchange a pair of equal sized subsets we have $A \cup B = A' \cup B'$. The first equality in the proposition results from the fact that $m(A \cup B, A \cup B) = m(A' \cup B', A' \cup B')$. Indeed we have

$$\begin{aligned} m(A \cup B, A \cup B) &= \sum_{s\in A\cup B} |\mathcal{N}_s \cap (A \cup B)| \\ &= \sum_{s\in A} |\mathcal{N}_s \cap (A \cup B)| + \sum_{s\in B} |\mathcal{N}_s \cap (A \cup B)| \\ &= \sum_{s\in A} |\mathcal{N}_s \cap A| + \sum_{s\in A} |\mathcal{N}_s \cap B| + \sum_{s\in B} |\mathcal{N}_s \cap A| + \sum_{s\in B} |\mathcal{N}_s \cap B| \\ &= m(A, A) + m(A, B) + m(B, A) + m(B, B). \end{aligned} \tag{59}$$

We have a similar equality for $m(A' \cup B', A' \cup B')$, establishing (57). The second equality in the proposition results from the fact that $m(A \cup B, C) = m(A' \cup B', C)$. Specifically,

$$\begin{aligned} m(A \cup B, C) &= \sum_{s \in A \cup B} |\mathcal{N}_s \cap C| \\ &= \sum_{s \in A} |\mathcal{N}_s \cap C| + \sum_{s \in B} |\mathcal{N}_s \cap C| \\ &= m(A, C) + m(B, C). \end{aligned} \tag{60}$$

Combining (60) with a similar equality for the primed sets gives (58). ∎

The first equality in the proposition can be construed as an *aura conservation principle*: when two disjoint sets exchange elements, the sum of their aura measures is conserved. Note that the neighborhood structure in these results could be arbitrary.

Also, consider the special case where $A_s = A$, $B_s = B$, and $|A| = |B|$. In this case, the two sets have completely exchanged places, and the aura conservation still holds. One could say that the lattice was "re-colored" by exchanging the colors of sets A and B.

The above results are valid for an arbitrary finite lattice. From now on, we need our usual assumption that that the finite lattice is rectangular with periodic boundary conditions. The neighborhoods of the lattice are assumed to be the translates of a structuring element $\mathcal{N}$.

The previous proposition was for disjoint sets A and B. When A and B also form a partition of the set $\mathcal{S}$, the aura measures,

$$m(A, A),\ m(B, B),\ m(A, B),\ m(B, A),$$

are related by the following proposition:

Proposition 19 *If $A \cup B = \mathcal{S}$ and $A \cap B = \emptyset$ then the following are true:*

$$m(A, A) + m(A, B) = |A||\mathcal{N}| \tag{61}$$

$$m(B, A) + m(B, B) = |B||\mathcal{N}|. \tag{62}$$

Proof: We will prove the first equality. The second could be proved in a similar way. From the definition,

$$\begin{aligned} m(A, A) + m(A, B) &= \sum_{s \in A} |\mathcal{N}_s \cap A| + \sum_{s \in A} |\mathcal{N}_s \cap B| \\ &= \sum_{s \in A} |\mathcal{N}_s \cap (A \cup B)| \quad \text{(because A,B are disjoint)} \\ &= \sum_{s \in A} |\mathcal{N}_s \cap \mathcal{S}| \\ &= \sum_{s \in A} |\mathcal{N}_s| \\ &= |A||\mathcal{N}|. \end{aligned} \tag{63}$$

∎

Corollary 20 *If the set A exchanges an element with its complement $A^c = B$, then*

$$\begin{aligned} & m(A', A') + m(B', B') + m(A', B') + m(B', A') \\ &= m(A, A) + m(B, B) + m(A, B) + m(B, A) \\ &= |\mathcal{S}||\mathcal{N}|. \end{aligned} \tag{64}$$

Proof: Notice first that if A and B form a partition of $\mathcal{S}$ then A' and B' also form a partition of $\mathcal{S}$ and $|A'|+|B'| = |A|+|B| = |\mathcal{S}|$. The corollary results from the two equalities in Proposition 19 applied to (A, B) and to (A', B'). ∎

If the boundary conditions were not assumed to be periodic, the right-hand sides in Proposition 19 and Corollary 20 would become upper bounds of the left hand sides. This follows from the observation that the sizes of neighborhoods at interior sites would become larger than those at boundary sites.

Corollary 20 also manifests an inverse relation between self-aura and cross-aura measures. Assume a symmetric neighborhood so that $m(A, B) = m(B, A)$. With the periodic boundary assumption,

$$m(A, A) + m(B, B) + 2m(A, B) = |\mathcal{S}||\mathcal{N}|. \tag{65}$$

If $|A|$ and $|B|$ are constant and nonzero, then as the self measures increase, the cross measures decrease, and vice versa. This behavior corresponds to our intuition: as set A clumps [6], and set B clumps, they separate themselves from each other. Because of our assumption of a connected lattice, as long as both A and B are present, there will also be some lower bound for $m(A, B)$ due to geometric constraints in the plane.

Example 21 *Consider the binary case with four nearest neighbors, where the colors clump into two regions on an $N \times N$ lattice. The boundary between the two regions will be as straight as possible, attaining in the limit a minimum length $m(A, B) = 2N$. Note that if we did not assume a periodic boundary, then the minimum length $m(A, B) = N$, since the regions would no longer share an edge along the lattice boundary.*

Examples of these minimum bounds, as well as images which illustrate these geometric constraints are provided in [30] where auras are applied to the study of the ground states of the Gibbs energy used in texture modeling.

G Generalized Isoperimetric Problem

Using a graph-theoretic point of view, (34) can be interpreted as a generalized isoperimetric problem. Following [9], we denote by $e(H, G)$ the edge boundary of a subgraph H in a graph G. An isoperimetric problem consists in finding

$$e(p, G) = \min\{e(H, G) \text{ such that } |H| = p\}. \tag{66}$$

If we think of the gray-level sets as subgraphs of the lattice graphs, then the uniform histogram constraint imposes a cardinality constraint similar to the one imposed in the isoperimetric problem. Moreover, we have seen in Section 3 that the aura measure is a generalization of the subgraph edge boundary. The cost function of (34) is a weighted sum of these generalized "edge boundaries," and therefore its minimization under the uniform histogram constraint can be construed as a generalized isoperimetric problem in the sense of [9]. These relations may make it possible to consider some network traffic and graph problems as problems in "pattern control".

References

[1] J. Besag, "Spatial interaction and the statistical analysis of lattice systems (with discussion)," *J. Roy. Stat. Soc., ser. B*, vol. 36, pp. 192–236, 1974.

[2] G. R. Cross, *Markov Random Field Texture Models.* PhD thesis, Michigan State Univ., 1980.

[6] In the condensed-matter literature, this same "clumping" behavior is referred to as "aggregation" or "coarsening".

[3] G. R. Cross and A. K. Jain, "Markov random field texture models," *IEEE T. Patt. Analy. and Mach. Intell.*, vol. PAMI-5, no. 1, pp. 25–39, 1983.

[4] P. A. Maragos and R. W. Schafer, "Morphological systems for multidimensional signal processing," *Proc. IEEE*, pp. 690–710, April 1990.

[5] S. Geman and D. Geman, "Stochastic relaxation, Gibbs distributions, and the Bayesian restoration of images," *IEEE T. Patt. Analy. and Mach. Intell.*, vol. PAMI-6, no. 6, pp. 721–741, 1984.

[6] R. Kindermann and J. L. Snell, *Markov Random Fields and their Applications*. Providence, Rhode Island: American Mathematical Society, 1980.

[7] D. H. Rothman and J. M. Keller, "Immiscible cellular-automaton fluids," *J. of Stat. Phys.*, vol. 52, no. 3/4, pp. 1119–1127, 1988.

[8] T. A. Witten, "Structured fluids," *Physics Today*, vol. 43, no. 7, pp. 21–28, 1990.

[9] B. Bollobás, *Combinatorics*. Cambridge: Cambridge University Press, 1986.

[10] S. Even, *Graph Algorithms*. Computer Science Press, 1979.

[11] P. Carnevali, L. Coletti, and S. Patarnello, "Image processing by simulated annealing," in *Proc. in Computer Vision* (M. A. Fischler and O. Firschein, eds.), Morgan Kaufmann, 1987.

[12] B. Julesz, "Visual pattern discrimination," *Proc. IRE*, vol. 8, no. 2, pp. 84–92, 1962.

[13] R. Haralick, "Statistical and structural approaches to texture," *Proc. IEEE*, vol. 67, pp. 786–804, May 1979.

[14] L. Van Gool, P. Dewaele, and A. Oosterlinck, "Texture analysis anno 1983," *Computer Vision, Graphics, and Image Processing*, vol. 29, pp. 336–357, 1985.

[15] L. S. Davis, S. A. Johns, and J. K. Aggarwal, "Texture analysis using generalized co-occurrence matrices," *IEEE T. Patt. Analy. and Mach. Intell.*, vol. PAMI-1, no. 3, pp. 251–259, 1979.

[16] A. Rosenfeld and A. C. Kak, *Digital Picture Processing, Volume 2*. Orlando: Academic Press, Inc., 1982.

[17] C. C. Gotlieb and H. E. Kreyszig, "Texture descriptors based on co-occurrence matrices," *Comp. Vis., Graph., and Img. Proc.*, vol. 51, pp. 70–86, 1990.

[18] R. W. Conners and C. A. Harlow, "A theoretical comparison of texture algorithms," *IEEE T. Patt. Analy. and Mach. Intell.*, vol. PAMI-2, no. 3, pp. 204–222, 1980.

[19] M. Hassner and J. Sklansky, "The use of Markov random fields as models of texture," *Comp. Graph. and Img. Proc..*, vol. 12, pp. 357–370, 1980.

[20] R. L. Kashyap and R. Chellappa, "Estimation and choice of neighbors in spatial-interaction models of images," *IEEE T. Inform. Theory*, vol. IT-29, no. 1, pp. 60–72, 1983.

[21] R. Chellappa and S. Chatterjee, "Classification of textures using Markov random field models," in *Proc. ICASSP*, (San Diego), pp. 32.9.1–32.9.4, 1984.

[22] L. Garand and J. A. Weinman, "A structural-stochastic model for the analysis and synthesis of cloud images," *J. of Climate and Appl. Meteorology*, vol. 25, pp. 1052–1068, 1986.

[23] H. Derin, H. Elliott, R. Cristi, and D. Geman, "Bayes smoothing algorithms for segmentation of binary images modeled by Markov random fields," *IEEE T. Patt. Analy. and Mach. Intell.*, vol. PAMI-6, no. 6, pp. 707–720, 1984.

[24] R. Chellappa, ""Two-dimensional discrete Gaussian Markov random field models for image processing"," in *Progress in Pattern Recognition 2* (L. N. Kanal and A. Rosenfeld, eds.), Elsevier Science Publishers B. V. (North Holland), 1985.

[25] H. Derin and H. Elliott, "Modeling and segmentation of noisy and textured images using Gibbs random fields," *IEEE T. Patt. Analy. and Mach. Intell.*, vol. PAMI-9, no. 1, pp. 39–55, 1987.

[26] A. Gagalowicz and C. Tournier-Lasserve, "Third-order model for non-homogeneous natural textures," in *Proc. Int. Conf. on Pattern Recog.*, 1986.

[27] C. Kittel and H. Kroemer, *Thermal Physics.* San Francisco: W. H. Freeman and Company, 1980.

[28] K. Huang, *Statistical Mechanics.* Wiley, 1963.

[29] R. J. Baxter, *Exactly Solved Models in Statistical Mechanics.* London: Academic Press, Inc., 1982.

[30] R. W. Picard and I. M. Elfadel, "Structure of aura and co-occurrence matrices for the Gibbs texture model," *J. of Mathematical Imaging and Vision*, vol. 2, pp. 5–25, 1992.

[31] R. W. Picard, *Texture Modeling: Temperature Effects on Markov/Gibbs Random Fields.* ScD thesis, M.I.T., 1991.

[32] R. W. Picard, I. M. Elfadel, and A. P. Pentland, "Markov/Gibbs texture modeling: Aura matrices and temperature effects," in *Proc. IEEE Conf. on Computer Vision and Pattern Recognition*, (Maui, HI), June 1991.